Characterizing Quantum-Dot Cellular Automata

Burkhard Ritter
Supervised by Prof. Kevin Beach

May 2014

Contents

Chapter 1

Quantum-dot cellular automata

1.1 An alternative computing paradigm

Lent *et al.* introduced the concept of quantum-dot cellular automata as an alternative computing paradigm in 1993 [1]. They devised a novel physical scheme to build digital circuits that would overcome some of the limitations of CMOS technology, promising potentially lower power consumption, higher device density, and faster clocking. As the name suggests, quantum-dot cellular automata (QCA) are made from quantum dots that are grouped into cells. Figure 1.1(a) shows a basic QCA cell in which four quantum dots are arranged on the corners of a square. The dots are idealized as perfectly localized single orbitals on a perfectly decoupled, non-intrusive medium. Because of the Pauli principle, each dot can be occupied by zero, one, or two electrons. In the QCA scheme, however, each cell is occupied by exactly two electrons in total and each constituent dot is quarter-filled on average. The electrons tunnel only weakly between different dots in a cell and the dominant energy scale is the Coulomb repulsion between the particles. Because of the large energy cost to two electrons occupying the same site or adjacent ones, the diagonal states are the two energetically preferred electron configurations. In comparison, edge states or doubly occupied quantum dots are unfavourable higher energy states, see Figure 1.1(b). The two diagonal states can be identified with logic 0 and 1, respectively. *A priori* the two bit encodings have the same energy, but this degeneracy can be lifted by an external Coulomb potential, arising, for example, from a second nearby QCA cell.

A single cell by itself is not very interesting. But multiple cells can be positioned next to one another, for example as a straight line of cells, as shown in Figure1.1(c). The approach once again assumes that Coulomb forces are strong and that electron tunnelling between cells is very small. For a straight line of cells, the long-ranged, unscreened Coulomb forces will tend to align the electron configurations of adjacent cells. If the first cell is in logic state 1, then the second cell will also prefer logic state 1 and so will in turn all the other cells in the line. The situation is the same for logic state 0. Therefore, a straight line of
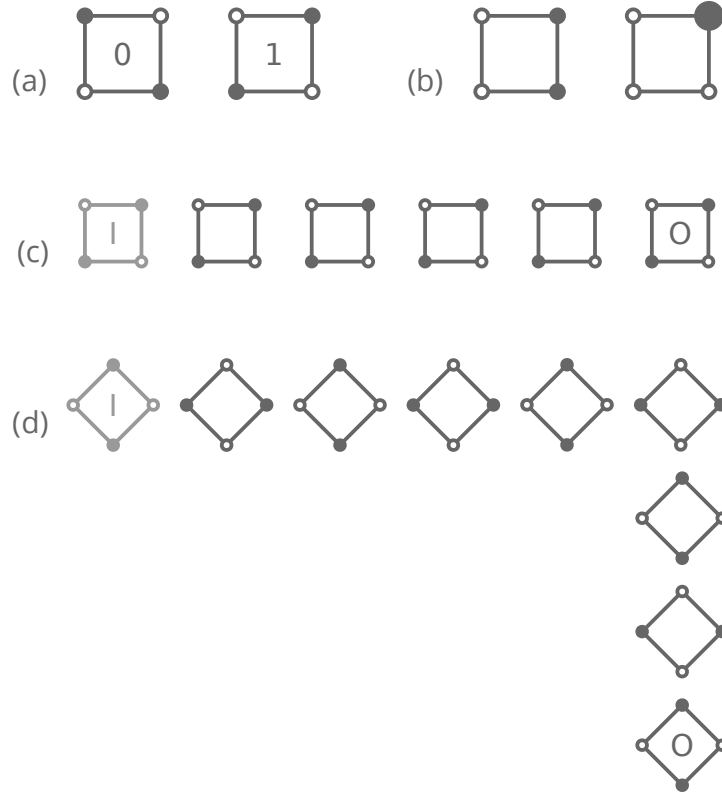
Figure 1.1: Building blocks of quantum-dot cellular automata (QCA). (a) A QCA cell consists of four quantum dots on the corners of a square and is occupied by two electrons. Due to Coulomb repulsion, two energetically preferred states emerge, logic 0 and logic 1. (b) Both electrons occupying the edge of the cell or doubly occupying a single quantum dot are unfavourable high-energy states. (c) A straight line of cells functions as a wire and transmits a signal. (d) A diagonal line of cells (cells rotated by 45°) transmits a signal alternating from cell to cell. Wires can have kinks.
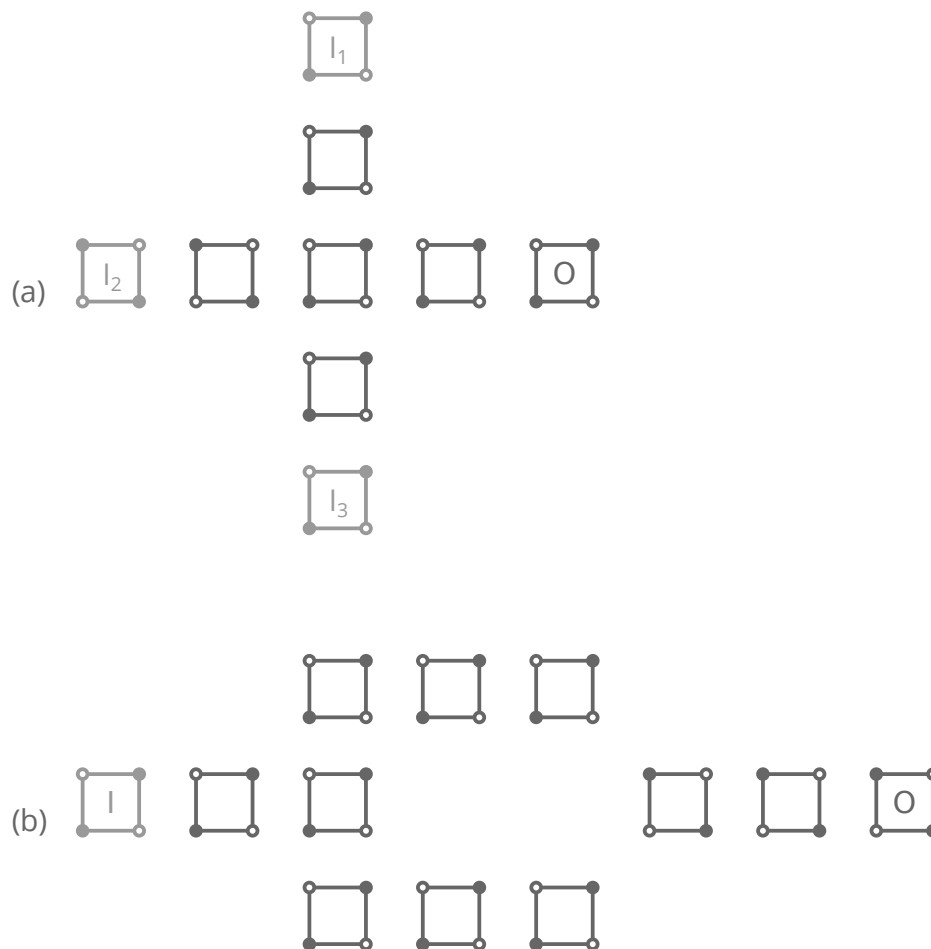
Figure 1.2: QCA gates. (a) The majority gate's three inputs "vote" on the output. The gate is commonly operated with one fixed input, for example I_3, and then functions as an AND ($I_3 = 1$) or OR gate ($I_3 = 0$) for the remaining two inputs. Here the gate performs the computation $1 \wedge 0 = 1$. (b) The inverter inverts a signal.

cells is similar to a wire not only in geometry, but also in functionality: it transmits a digital signal. The same is true, with slight modifications, for a diagonal line of cells—cells rotated by $45°$, as illustrated in Figure 1.1(d). In this case, the signal alternates from cell to cell, that is, logic 1 will follow logic 0 which followed from logic 0, and this again is simply by virtue of the dominant Coulomb interaction between electrons on different cells. By using an even number of cells the diagonal line of cells works as a wire just as well as a straight line of cells. The pictogram also demonstrates a $90°$ kink for the diagonal line of cells which our newly gained intuition for these Coulomb-driven systems expects to pose no problem for signal transmission.

The main idea of the QCA approach becomes apparent: Ideal, bistable cells interact with each other solely by Coulomb repulsion. By arranging the cells in clever geometries, we can realize interesting functionalities. The idea as such is quite general and does not strictly rely on the two-electron–four-dot cell introduced above. Indeed, a number of variations exist, such as cells consisting of two dots and occupied by only one electron that interact via dipole fields instead of quadrupole fields as for the conventional cells. Another variation is a four-dot cell with six electrons—two holes—instead of two electrons. Even the interaction need not be Coulombic. For example, magnetic QCA schemes have been explored [2]. While QCA carries "quantum" in its name and is sought to be implemented at the nanoscale, the approach operates close to the classical limit. The Coulomb interaction dominates with the tunnelling of electrons serving as a small perturbation, which nonetheless drives the system's dynamics. The approach is insensitive to the spin degrees of freedom. Let us finally note that QCA is a not a cellular automata in a strict mathematical sense, but only by analogy to the idea of interacting cells.

One clever geometrical cell arrangement, the majority gate, is shown in Figure 1.2(a). The gate has three inputs which "vote" on the central cell. The majority wins and sets the single output. The device is commonly operated with one fixed input, for example $I_3 \doteq 0$ or $I_3 \doteq 1$. In the first case, with $I_3 \doteq 0$, the device functions as an AND gate for the remaining two inputs, $O = I_1 \wedge I_2$. In the second case, with $I_3 \doteq 1$, it is an OR gate with $O = I_1 \vee I_2$. The figure shows the gate performing the computation $1 \wedge 0 = 1$. Now the only missing piece for Boolean algebra is negation, $O = \neg I$. We had already seen that simply arranging cells at an $45°$ angle as in the diagonal line of cells negates the signal from cell to cell. The inverter, shown in Figure 1.2(b), recasts this idea into a more robust layout. With that we have, at least in principle, all the necessary building blocks for Boolean algebra and thus digital circuitry.

Conceptually, it is most elegant to set the inputs for a QCA circuit via driver cells—cells that resemble the QCA cell in form, but are made up of static point charges instead of quantum dots. These static charges are thought to be manipulable to vary the input smoothly from the logic 0 to the logic 1 state. In Figures 1.1 and 1.2, these driver cells are represented in light grey. Of course, in practice such driver cells would be difficult if not impossible to implement and the inputs are more likely set by leads that provide the necessary perturbative electrostatic fields. The output of a QCA device can be directly

read from its output cells. In practical implementations this will require a non-trivial charge probing apparatus. Changing the input for a QCA device throws the system into an excited, non-equilibrium state. The system will then dissipatively propagate to its new ground state. For the given inputs, this ground state corresponds to the solution of the computational problem the circuit is designed to solve. Let us emphasize this: in QCA, the computational solution maps directly to the physical ground state. While the computation is being performed, only a few charges move locally, in each cell. Operating close to the ground state, QCA is thus a truly current-free approach and consequently inherently low-power, especially when compared with CMOS technology. But the operation close to the ground state also raises concerns for the operational temperature for these devices. It is clear that for applications we would want to engineer the system so that the energy gap between the ground state and the low-lying excited states far exceeds room temperature. Different material systems provide different dissipative channels, and modelling them quantitatively or even qualitatively correctly is very challenging. As a consequence, it is difficult to derive general expectations for the clocking speed of QCA circuits. The switching speed of a majority gate, for example, will greatly depend on the system's parameters, but particularly on the nature of the dissipative coupling of the circuit to its environment. A small dissipative coupling will have the output polarization oscillating before it eventually settles to its correct value. A very dissipative system in contrast might get stuck in meta-stable states.

QCA circuits consist of wires, gates, and other structures arranged on a two-dimensional surface—very similar to conventional electronics devices. However, the structures themselves are quasi-one-dimensional and this poses a challenge for building large-scale QCA circuits. A good example is a single long wire, which is truly one-dimensional. When we think about switching the input for the wire, we think of the information being propagated as a charge density wave along the line of cells, or, equivalently, as propagating the domain boundary between logic 0 and logic 1. This domain boundary incurs an energy cost that the system seeks to minimize, causing the wire to order. For an increasingly longer wire, however, the gain in entropy for moving a domain boundary freely throughout the wire ($S \sim \log N$, N the number of cells) soon exceeds the loss in energy, which is reflected by the free energy of the system ($F = U - TS$). Quite generally, a one-dimensional system cannot be ordered in the thermodynamic limit except at zero temperature. Therefore, the finite-temperature, infinitely long wire will always exhibit exponentially decaying bit correlations and thus not be able to transmit a signal. The gap between the first excited state—with two domains—and the completely ordered ground state, together with the desired operational temperature will determine the maximum system size.

To address this scaling problem, we partition large circuits into smaller units. The size of each unit is chosen to be small enough to avoid entropy-induced disorder at a given operational temperature. Each unit can be turned "on" and "off" separately: ideally, individual gates would allow one to effectively raise and lower the tunnelling barriers between quantum dots in each unit and thus provide a mechanism to freeze or delocalize
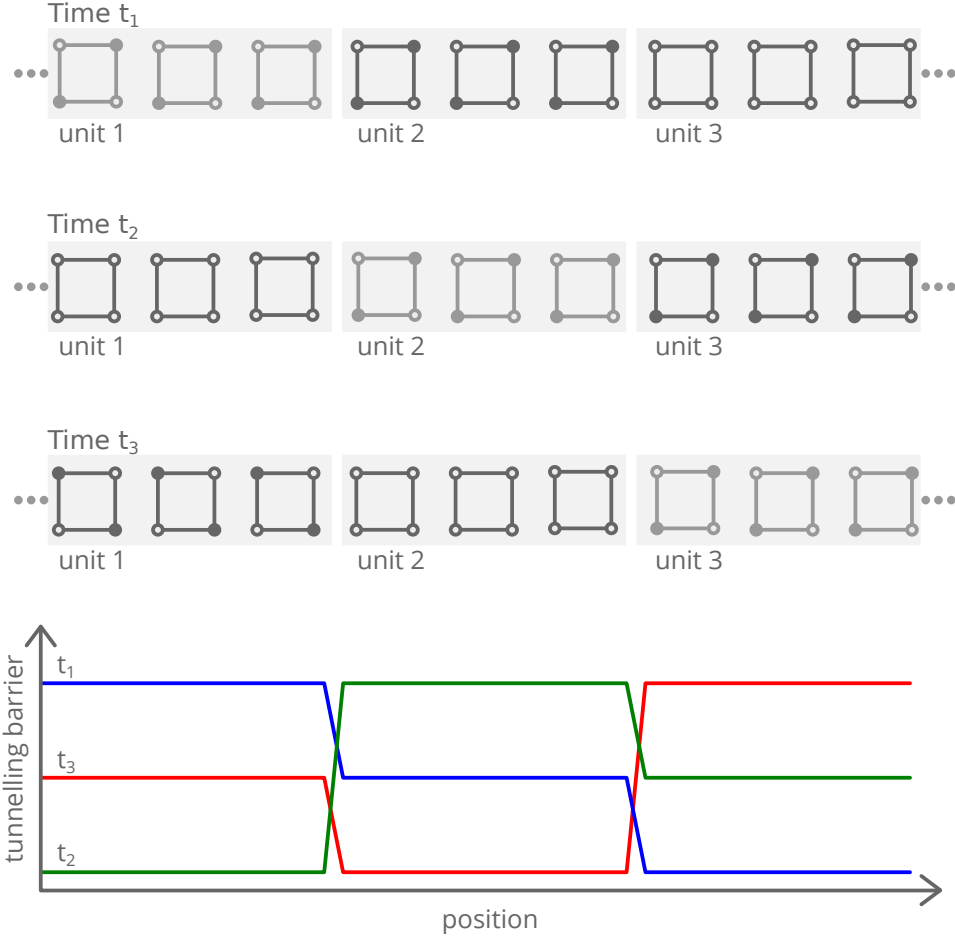
Figure 1.3: Clocked QCA for a line of cells. To avoid entropy-induced disorder in large QCA circuits, the system is partitioned into smaller units, labelled 1, 2, and 3 in this example. By varying the tunnelling barriers, each unit is put through the three phases *frozen* (high barrier, light grey cells), *active* (medium barrier, dark grey cells), and *delocalized* (low barrier, dark grey cells with empty dots). Synchronizing the phases of adjacent units allows to pipeline information flow and computations. The line of cell's three units and their tunnelling barriers are shown at three different times, $t_1 < t_2 < t_3$. A logic 1 state is propagated from the left to the right. At t_3 a logic 0 state is coming in from the left.

the electrons. A unit with *frozen* electrons can serve as the input for a unit with more *active* charge carriers, which works like a regular QCA circuit. A unit with completely *delocalized* electrons, in contrast, will not influence adjacent units. By putting each unit through the three phases *delocalized*, *active*, and *frozen* and synchronizing adjacent units appropriately, we can control the information flow through the system very nicely, as illustrated in Figure 1.3. Therefore, by partition the circuit and introducing a clocking scheme we not only handle the scaling problem, but also arrive at a pipelining architecture. If and how the tunnelling barriers can be effectively modified will depend on the details of the specific QCA implementation. Also, in practice the QCA circuit units cannot be too small as they must be individually addressable. Gates which turn QCA units "on" and "off" provide another potential benefit as well. We are able to control how and especially how fast the gate voltage is changed and should be able to tune it with respect to the inherent time scales of the QCA system, which are set by the system's parameters and the dissipative coupling to its environment. This should afford a better control over the dynamics of the switching process and might help mitigate problems such as oscillating outputs and meta-stable states, mentioned above [3].

1.2   Atomic silicon quantum dots

Our objective is the general, rather than implementation-specific, characterization of the QCA approach. Even so, it is still important to consider concrete experimental realizations, not only as a motivation for our work, but also to put our modelling and results into context. One of the most promising and recent experimental implementations of QCA is based on atomic silicon quantum dots, and we will therefore use them as our experimental reference. Atomic silicon quantum dots were first demonstrated as a possible QCA implementation by Wolkow *et al.* in 2009, when the group first constructed one single QCA cell. Figure 1.4(a) shows a scanning tunnelling microscope (STM) image of their device. Since then impressive advances have been made both in the understanding of the electronic properties of these quantum dots as well as in the precise fabrication of larger QCA structures. With atomic-scale feature sizes, this experimental system promises room temperature operation, while at the same time tapping into the established and highly sophisticated silicon technology. Being based on silicon should also ease integration with existing CMOS circuitry.

Atomic silicon quantum dots are *dangling bonds* on a hydrogen-terminated (100) silicon surface. Atoms on a (100) silicon surface have two unsatisfied bonds. Pairs of surface atoms form dimers, satisfying one bond. The remaining bond is satisfied by passivating the surface with hydrogen. Figure 1.4(c) shows a STM image of the reconstructed silicon surface, where the dimer rows are clearly visible and the dimensions are indicated. By applying a relatively large current through the STM tip, individual hydrogen atoms can be removed, with atomic precision. This leaves a *dangling bond* (DB) that acts as a quantum dot: energetically, electrons on the DB orbital sit in the silicon band gap and are therefore

(a)

(b)

CB — 1.12 eV
- - - - - 1.05 eV
0.85 eV

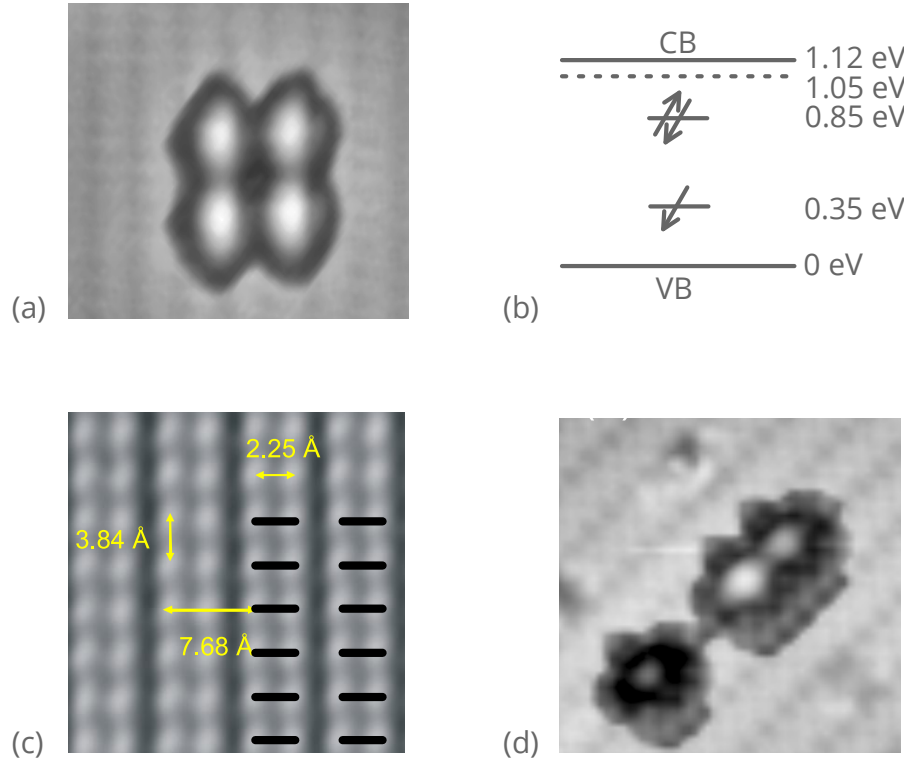0.35 eV

0 eV
VB

(c)

2.25 Å

3.84 Å

7.68 Å

(d)

Figure 1.4: Atomic silicon quantum dots are *dangling bonds* (DBs) on a hydrogenated (100) silicon surface. (a) A scanning tunnelling microscope (STM) image of an atomic silicon quantum dot QCA cell. (b) Band diagram of a DB on a strongly n-doped silicon substrate. (c) The reconstructed (100) hydrogenated silicon surface, showing dimer rows. (d) Two closely spaced tunnel-coupled DBs perturbed by a third DB. The top right DB is seen to be more negatively charged than the other DB of the closely spaced pair, due to Coulomb repulsion from the perturbing third DB in the bottom left. All STM images and *ab initio* estimates from Wolkow *et al.* [4] [5].

decoupled from the silicon substrate. Figure 1.4(b) shows the band diagram of a DB on an n-doped substrate. Chemically, DBs have proven to be surprisingly robust with respect to environmental molecules. From *ab initio* calculations it is known that the sp^3 DB orbital extends predominantly into the bulk and only a little into the vacuum. The orbital's lateral extent is on the order of 1 nm and therefore spans multiple silicon lattice atoms. Due to orbital overlap, closely spaced DBs are tunnel-coupled. A neutral DB consists of the positive silicon ion and one electron. In the experimentally common strongly n-doped system, the DB accepts one more electron and is therefore $-1e$ negatively charged. Conversely, in a p-doped sytem the DB will donate its electron and become $+1e$ positively charged. The Coulomb repulsion between negatively charged DBs can be used to adjust the filling of DB assemblies simply by controlling the DBs' positions. For example, on an n-doped substrate two DBs may eject one electron (which goes back to the bulk) and share the remaining single electron, when placed close enough together. To prove this, a third DB is placed close by, but not close enough to be tunnel-coupled. The effect of the Coulomb repulsion can be seen via STM imaging, Figure 1.4(d), where the DB farthest from the perturbing external charge is more negatively charged (darker in the STM image) than the closer DB. The observed charge shift is only possible when both closely-spaced DBs share a single electron. To form the previously shown QCA cell, Figure 1.4(a), on a strongly n-doped silicon substrate four DBs are brought close enough together so that two electrons go back to the bulk, leaving the cell with six electrons (two holes) in total and a cell net charge of $-2e$, which is the right charge regime for QCA.

Atomic silicon quantum dots provide some examples of how a real world system might be different from the idealized picture we typically employ to describe the QCA approach. We like to think of quantum dots as perfectly localized orbitals. But in the silicon system the orbitals of the DBs actually span multiple lattice sites and only if the DBs are placed far enough apart might we still be able to consider them as localized. We do not consider the substrate but treat quantum dots as perfectly isolated entities. Of course, in practice the substrate will certainly influence the QCA device. In the silicon system free charge carriers will screen the long-ranged Coulomb interactions that the QCA scheme relies on, although likely on scales larger than the circuit feature size. The screening is not necessarily disruptive for QCA and might even be beneficial, for example by minimizing charge-buildup in large systems. But to quantify the screening accurately it is necessary to thoroughly understand and precisely model the system in detail which, for atomic silicon quantum dots which live at the surface, would surely be very challenging. The silicon substrate could also, conceivable, provide a second tunnelling channel between DBs. In addition to electrons hopping directly from DB to DB they could first tunnel from the first DB to the substrate and then back to the second DB. Therefore an accurate model for atomic silicon quantum dots might need to accommodate the nature of the DB orbitals, screening, multiple tunnelling channels and possibly other effects.

1.3   The extended Hubbard model

QCA systems are typically modelled by an extended Hubbard Hamiltonian. The Hubbard model originated in the early 1960s to describe rare-earth systems with highly localized d- and f-electrons and has since then, of course, become one of the most widely studied and successful models in condensed matter physics [6]. In basing our description on the Hubbard model we already put some key assumptions in place. For example, we assume that the quantum dots are similar to the highly localized d-orbitals. As discussed above, depending on the particular QCA implementation this might or might not be a good description. However, our interest is not in the precise details of any particular material system, but our aim is to investigate universal characteristics of QCA systems. As long as a QCA system can be broadly qualitatively described by Hubbard physics—and most prospective QCA implementations fall into this category—our modelling and findings should be valid. Conversely, for implementations that are decidedly not Hubbard-like, our results might not be applicable. An idealized but semi-realistic description is what we want and for that the Hubbard model is indeed an appropriate—and tractable—starting point. Specifically, the Hamiltonian we use is

$$
\begin{aligned}
H = &- \sum_{ij\sigma} t_{ij}\, c_{i\sigma}^{\dagger} c_{j\sigma} + U \sum_{i} n_{i\uparrow} n_{i\downarrow} - \mu \sum_{i\sigma} n_{i\sigma} \\
&+ \sum_{i<j} V_{ij} \left(n_{i\uparrow} + n_{i\downarrow} - q \right) \left(n_{j\uparrow} + n_{j\downarrow} - q \right),
\end{aligned}
\tag{1.1}
$$

where $c_{i\sigma}^{\dagger}$ ($c_{i\sigma}$) creates (annihilates) an electron on quantum dot i with spin σ and the particle number operator is $n_{i\sigma} = c_{i\sigma}^{\dagger} c_{i\sigma}$. The overlap integral between dots i and j is denoted by t_{ij}, U is the Hubbard on-site Coulomb repulsion, μ the chemical potential, and V_{ij} the long-ranged Coulomb interaction, which is characteristic for QCA systems. For simplicity the Coulomb term is chosen to be $V_{ij} = \frac{1}{r_{ij}}$ where r_{ij} is the distance between the two dots i and j. We also introduce the *compensation charge* q which is thought to represent a possible positive ion at each quantum dot site. This constant positive charge allows us to tune the net cell charge. For two electrons per cell, for example, $q = 0$ yields a net cell charge of $-2e$ whereas $q = \frac{1}{2}$ represents zero net cell charge. The $q = \frac{1}{2}$ charge neutral cells are perfect electrostatic quadrupoles.

The geometric layout of the QCA system and therefore its functionality is encoded in the hopping parameter t_{ij} and the long-ranged Coulomb term V_{ij}. For the hopping parameter we usually only consider nearest-neighbour hopping t and specifically no hopping between the cells. While this constraint is not strictly necessary for QCA, it is in line with the approach's underlying idea and greatly simplifies calculations. Because the overlap integral decays exponentially with distance, as long as the distance between dots from different cells is larger than the distance between dots within one cell, the assumption will introduce only a small error. Still, this is something to keep in mind if we place
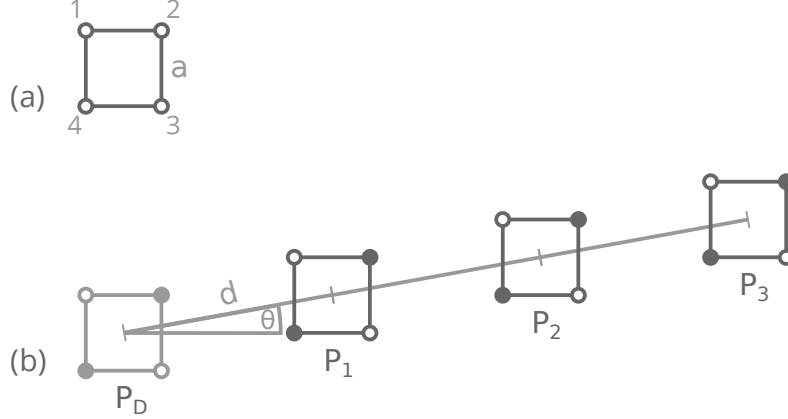
Figure 1.5: Parameterizing QCA layouts. (a) The edge length of a QCA cell is denoted by a. The dots of each cell are numbered clockwise. (b) A three-cell wire. The cell-cell distance is denoted by d, the cell-cell angle by θ. The wire's input is set by the driver cell's polarization P_D, the active cells' polarizations are P_1, P_2, and P_3.

cells very close to each other. Note that without inter-cell hopping we can decompose the Hamiltonian into purely Coulombic cell-cell interaction terms H_{kl}^{cc} and single cell terms H_k^c, which capture the kinetics as well as the inside-cell Coulomb interactions,

$$H = \sum_k H_k^c + \sum_{k<l} H_{kl}^{cc} \, , \tag{1.2}$$

where k and l number the cells.

To parameterize the Coulomb term V_{kl} and specifically r_{ij}, the distance between quantum dots i and j, we introduce the cell edge length a and the cell-cell distance d, as illustrated in Figure 1.5(a) and (b) where we have used a short line of cells as an example QCA system. The angle between adjacent cells is denoted by θ. Ideally each cell should be in logic state 0 or logic state 1, but, of course, in practice a cell can be in any superposition of the two states or even in a different state altogether. The *cell polarization P_k* quantifies the state of the cell,

$$P_k = \frac{1}{2} \left(n_{4k+2} + n_{4k+4} - n_{4k-1} + n_{4k-3} \right) \, , \tag{1.3}$$

where the dots in each cell are numbered clockwise as indicated in the figure. We have also introduced the shorthand notation $n_i = n_{i\uparrow} + n_{i\downarrow}$. The cell polarization is $P_k = -1$ for a logic 0 and $P_k = +1$ for a logic 1 state. Without any external input the polarization of a cell will be $P_k = 0$. In the example line of cells, the input is set via the driver cell's polarization P_D at the left end. The driver cell's four static point charges are adjusted to

reflect the desired polarization P_D. For QCA, the cell polarization really is the observable of utmost interest. It indicates whether a cell is more in logic state 0 or logic state 1 and how polarized the cell is, where ideally it should always be fully polarized, $|P_k| = 1$. In short, the cell polarizations will indicate how well the QCA approach works for a given system and, unsurprisingly, calculating cell polarizations for various geometric layouts over a wide range of system parameters will be our main focus.

The QCA cell is characterized by three energy scales: the nearest-neighbour hopping t, the nearest-neighbour Coulomb repulsion $V_1 = \frac{1}{a}$, and the on-site Coulomb repulsion U. For QCA operation, U is usually assumed to be sufficiently large so that doubly occupied states are gapped out. We can introduce $V_0 = \frac{1}{\sqrt{2}a}$, the next-nearest-neighbour Coulomb repulsion, which corresponds to both electrons sitting on the diagonal of the cell—our preferred $P_k = \pm 1$ states, ideally the ground state. Conversely, V_1 corresponds to both electrons occupying the edge of the cell. Again, for QCA operation we would like the edge states to be sufficiently gapped out. In other words, the energy gap ΔV,

$$\Delta V = V_1 - V_0 = \frac{2 - \sqrt{2}}{2} \frac{1}{a} \approx 0.3 V_1 \,, \tag{1.4}$$

should be large compared to temperature $\Delta V \gg T$, and similarly $U \gg \Delta V \gg T$. The competition between temperature T and V_1 will thus directly influence how polarized a cell is. In addition, V_1, which seeks to order the cell, will compete with t, which delocalizes and disorders the electrons. QCA is thought to function in a regime where Coulomb is the dominating energy scale and hopping is a small perturbation: the ratio $\frac{V_1}{t}$ is large. But it is also clear that if $\frac{V_1}{t}$ becomes too large, for example by taking $t \to 0$, the system slows down and eventually freezes, which is rather undesirable for QCA operation as well. In essence we can describe a cell by the ratios $\frac{V_1}{t}$, $\frac{U}{t}$, and $\frac{T}{t}$. By similarly expressing the cell-cell distance in units of the cell size $\frac{d}{a}$, we characterize any QCA system in dimensionless units.

1.4   Basic characterization

At the time of this writing, the QCA idea is over twenty years old. Naturally, the fundamental building blocks of QCA circuitry such as the single cell itself, the wire, and the majority gate have been characterized. Interestingly, time-independent properties were investigated relatively briefly and arguably not exhaustively. The bulk of the existing theoretical work soon focused on system dynamics, building large scale computing architectures with the QCA paradigm, and on specific potential experimental implementations. Previous work on the characterization of time-independent QCA properties yielded two main results. First, the cell-cell response, that is, how the polarization of one cell responds to the polarization of a neighbouring cell, was established to be non-linear and exhibit gain [1]. Therefore, even an only partially polarized cell would fully polarize the cell next to it, Figure 1.6(a). Of course, gain is highly desirable, if not essential, for building digital circuits. It compensates
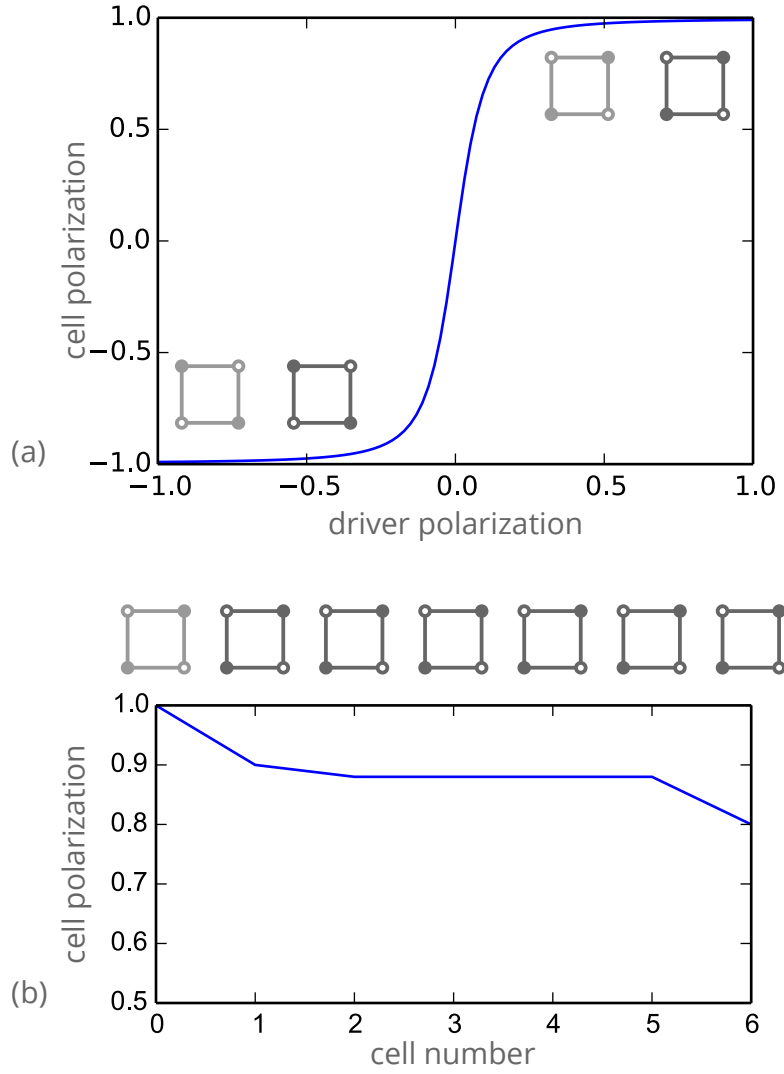
Figure 1.6: Basic characteristics of QCA devices, schematically. (a) The response of a cell's polarization to a driver cell's polarization is non-linear and exhibits gain. This gain has been used extensively to argue for the QCA approach's inherent robustness. (b) Cell polarizations of a six-cell wire with input polarization $P_D = 1$, as calculated with the intercellular Hatree approximation. Most cells are polarized with the same saturation polarization and only the leftmost and rightmost cells deviate slightly. In this picture, the output polarization does therefore not depend on the wire length.

any loss or imperfections and makes the scheme overall robust. Not coincidentally, CMOS technology is built around the MOSFET transistor with gain as one of its intrinsic properties. Second, lines of cells were seen to be polarized with an almost constant polarization throughout the whole line, Figure 1.6(b) [7]: apart from a few cells next to the driver cell, all remaining cells in the line would be polarized with the same *saturation polarization*. As a consequence, the output polarization should not depend on the number of cells in the line. The saturation polarization was observed to be largely independent of the driver cell's polarization, but solely determined by the system's parameters such as the hopping t and the Coulomb energy V_1. For unfavourably chosen parameters the saturation polarization might be very small, but over a wide range of system parameters it was shown to be close to perfect. For example, for large hopping t the saturation polarization is expected to be zero. If t is then decreased and passes a critical point t_c, a second-order phase transition takes place. The saturation polarization becomes non-zero and in fact very quickly close to perfect as t is further decreased. In addition to the cell-cell response and the analysis of a line of cells, larger QCA structures such as the majority gate were reported to function correctly for a select set of parameters, but were not analyzed in depth. Overall, the physical picture emerging from the early time-independent calculations is of bistable cells readily snapping into the correct fully polarized state throughout the whole device. It is a picture where the QCA approach works robustly and in fact almost perfectly over a presumably wide range of parameters. It is the prevailing picture to this day. It is also quite wrong.

These early calculations of time-independent QCA properties concentrated almost exclusively on the ground state of the system (with one exception [8]). However, focusing solely on the ground state is not sufficient. While the QCA approach is intended to be operated "close to the ground state," at least the first excited state is needed to obtain an estimate for the operational temperature for these devices—a parameter of significant practical interest. More subtly, what the QCA idea calls ground state actually corresponds to multiple states, namely one spin singlet and three spin triplet states for $P = -1$ and $P = 1$, respectively, in a single cell. While these states can reasonably be expected to be near-degenerate, a thorough study of QCA should still consider them. In more practical terms, QCA is expected to operate at finite temperatures so simulating the devices at non-zero temperature just makes sense. Similarly, the existing work on time-independent QCA properties is not exhaustive in the exploration of other parameters. For example, while the saturation polarization's dependence on V_1 and t is mapped out, concrete numerical values for these quantities are hard to come by. In other cases the Coulomb scale V_1 is not indicated explicitly at all. Cells are assumed to be charge-neutral, but the effects of non-charge-neutrality are not investigated. Different cell-cell distances are not discussed, nor what system parameters should be chosen for optimal performance.

The exact numerical simulation of QCA systems is challenging and in fact intractable for all but the smallest structures. Therefore, approximations are necessary. In the literature on QCA two approximations are prevalent: the intercellular Hartree approximation (ICHA) and the two-states-per-cell approximation [1] [9]. Most of the studies of time-independent

QCA properties employ the ICHA. Only the cell-cell response is calculated with a "full" quantum mechanical model, where the "full" model is actually already the reduced Hilbert space of exactly two electrons per cell. ICHA is a mean field scheme: the Hamiltonian of one cell is solved exactly in the mean field of the polarizations of all the other cells. More specifically, the cell-cell interaction term H_{kl}^{cc} in equation (1.2) is rewritten

$$
\begin{aligned}
H_{kl}^{cc} &= \sum_{\substack{i \in k \\ j \in l}} V_{ij} \left(n_i - q\right) \left(n_j - q\right) \\
&\approx \sum_{\substack{i \in k \\ j \in l}} V_{ij} \left[\left(n_i - q\right)\left(\langle n_j \rangle - q\right) + \left(\langle n_i \rangle - q\right)\left(n_j - q\right)\right] ,
\end{aligned}
\tag{1.5}
$$

and, introducing the mean field for dot i on cell k,

$$
\tilde{V}_i^k = \sum_{l \neq k} \sum_{j \in l} \left(\langle n_j \rangle - q\right) = \sum_{l \neq k} \mathcal{F}\left[\langle P_l \rangle\right] ,
\tag{1.6}
$$

the one-cell mean field Hamiltonian becomes

$$
H_k^{\mathrm{MF}} = H_k^c + \sum_{i \in k} \left(n_i - q\right) \tilde{V}_i^k .
\tag{1.7}
$$

Because the cell polarization is directly related to the occupancies of the sites of the cell, we have $\tilde{V}_i^k = \tilde{V}_i^k(\langle P_l \rangle)$. Solving the one-cell Hamiltonian allows one to compute to polarization $\langle P_k \rangle$ of the cell, which in turn is used to set the mean field originating from all other cells. The procedure is repeated until a self-consistent cell polarization and thus self-consistent solution for Equation (1.7) is found. By using $n_i n_j \approx n_i \langle n_j \rangle + \langle n_i \rangle n_j$ mean field approximations neglect quantum fluctuations. Only at high dimensionality can these fluctuations really average to zero, and indeed mean field schemes can be shown to become exact in the limit of infinite dimensionality [10]. Conversely, for low dimensional systems fluctuations are more important and mean field approximations are intuitively expected not to work very well. As an uncontrolled approximation, the validity of a mean field approach has to be verified on a case by case basis. Consequently, because QCA is quasi-one-dimensional, it is arguably not well suited for a mean field treatment. Even then a mean field approximation might be appropriate as a first stab at the problem. But ICHA, having been introduced in the very first QCA paper, was never verified or complemented by more accurate methods. It is rather remarkable that a large part of the existing work on QCA characterization rests, directly or indirectly, on an approximation that can reasonably be expected to give wrong results. And indeed, in the context of the dynamic properties of QCA it has been known for a long time that ICHA does go wrong [11]. Much more recently, it has been shown very explicitly that even for the single cell-cell response ICHA introduces artefacts that are clearly non-physical [12]. As an intuitive simple example

where ICHA will give wrong results we can go back to the infinitely long wire we already discussed above: we argued that due to entropy the infinite wire can only be ordered at zero temperature. In contrast, a mean field approximation will predict order up to a finite critical temperature.

For the calculation of time-dependent properties, the two-states-per-cell approximation is typically used, precisely because it was realized that ICHA is not sufficient, for example to calculate the switching behaviour of some majority gate structures. Perplexingly, in the literature the two-state approximation is motivated and justified by the ICHA picture [9]. Starting from the observation that cells in a wire are polarized with a saturation polarization P_{sat}—in ICHA calculations—a cell is represented by two basis states, corresponding to $P = P_{sat}$ and $P = -P_{sat}$. In a loose sense, the two-states-per-cell model thus comes from a picture of how we would like QCA to work: perfectly bistable, interacting cells. The approximation has been verified to the extent that it was shown that the ground state of the full quantum mechanical model can be represented nearly perfectly by the two-state basis, but only for one cell and for one particular set of system parameters. In a more rigorous treatment it should be possible to clearly derive the two-state model as the correct emerging low-energy Hamiltonian from the original extended Hubbard model. Such a derivation would also work out the parameter regime where the effective two-state Hamiltonian is valid. We will attempt the derivation in due course. In contrast to ICHA the two-states-per-cell approximation retains inter-cell entanglement and therefore yields more correct results, not only for dynamics, but also for time-independent properties. This comes at the cost of exponential scaling for the two-state model, whereas ICHA scales linearly in system size. Therefore, even with the two-state approximation only relatively small QCA devices are computationally feasible. As a final note, the two-state model is clearly very similar to a transverse field quantum Ising model, where the two polarization states correspond to a pseudo spin and the hopping is like a transverse field, flipping cell polarizations.

1.5   Exact diagonalization

We use the exact diagonalization numerical method [10] to simulate QCA systems described by the Hamiltonian (1.1). In principle, exact diagonalization is a straightforward method: for a chosen basis the matrix of the Hamiltonian is constructed explicitly and then diagonalized, yielding the eigenenergies and eigenstates of the system. With that we know everything about the system and can calculate observables of interest. The problem is that memory consumption scales as N_s^2 and the computational cost roughly as N_s^3, where N_s is the size of the state space; and the number of states scales exponentially with system size, $N_s = 4^{N_d} = 256^{N_c}$. N_d denotes the number of dots and N_c the number of cells. As an example, to store the full Hamiltonian matrix of a two cell QCA system requires 3GB of memory, to store the Hamiltonian matrix of a three cell system already requires 2000TB.

That's clearly not feasible on any available computer. As a side note, we cannot employ projective algorithms like Lanczos [10], because we are interested in finite temperatures and therefore need the full energy spectrum. Typically, projective schemes are only useful to calculate the ground state or the few lowest energy states.

To decrease the memory requirements and computational cost of exact diagonalization, symmetries must be exploited. The Hamiltonian matrix is actually quite sparse—most entries are zero. By using symmetries and a suitable basis, the Hamiltonian matrix can be brought into block diagonal form and then only those much smaller blocks need to be diagonalized. Our QCA system is symmetric with respect to the total particle number $\hat{N} = \sum_i \hat{n}_{i\uparrow} + \hat{n}_{i\downarrow}$ and the total spin $\hat{S} = \sum_i \hat{n}_{i\uparrow} - \hat{n}_{i\downarrow}$, i.e. $[\hat{N}, \hat{H}]_- = [\hat{S}, \hat{H}]_- = 0$. If we now use basis states which are eigenstates of the symmetry operators, $|n, s, l\rangle$, with

$$\begin{aligned}
\hat{N} |n, s, l\rangle &= n |n, s, l\rangle \ , \\
\hat{S} |n, s, l\rangle &= s |n, s, l\rangle \ ,
\end{aligned} \tag{1.8}$$

then we have

$$\begin{aligned}
\langle n', s', l' | [\hat{N}, \hat{H}]_- | |n, s, l\rangle &= (n' - n) \langle n', s', l' | \hat{H} |n, s, l\rangle \overset{!}{=} 0 \\
\langle n', s', l' | [\hat{S}, \hat{H}]_- |n, s, l\rangle &= (s' - s) \langle n', s', l' | \hat{H} |n, s, l\rangle \overset{!}{=} 0
\end{aligned} \tag{1.9}$$

and therefore

$$\langle n', s', l' | \hat{H} |n, s, l\rangle = 0 \qquad \text{for } n \neq n' \text{ or } s \neq s' \ . \tag{1.10}$$

Consequently, by ordering basis states by the symmetry operators' eigenvalues the Hamiltonian matrix becomes block diagonal, where the blocks are labelled by n and s. The blocks can be constructed and diagonalized separately and all observables can then be calculated block-wise as well, hence vastly reducing memory requirements and computational time. In our implementation, however, we do keep all blocks in memory simultaneously. This still yields considerably reduced memory usage and the same speedup in computational time. For the QCA system the single largest block is the spin zero sector at half-filling. Its size is

$$N'_s = \binom{N_d}{\frac{1}{2}N_d}^2 . \tag{1.11}$$

This corresponds to memory requirements of 180MB for two cells and 5400GB for three cells. Thus, although this is a considerable improvement for the two cell system (not least in computational time), the three cell system still remains unreachable with conventional computer hardware. To access larger systems we need to introduce approximations, which we will pursue in detail and with great care in the following chapter.

Computational physics is, true to its name, to considerable extent concerned with writing computer code. If ingenious algorithms which bring sophisticated physical problems to the computer are the art that excites the computational physicist's intellect, then writing

good computer code is the craft. It is a curious fact that traditionally in computational condensed matter physics, little weight has been put on collaboration on the code level, the development of common tools, coding techniques, and the code itself. This not only frustrates the newcomer to the field, for it is a long way from a formally stated algorithm to a correct and efficient implementation, but also poses a more fundamental problem to science in a time when computing has long become an essential part of it. Scientific results obtained from sophisticated numerical algorithms can be difficult to verify and reproduce without an openly available implementation of those algorithms. But verification and reproducibility are core assets of the scientific process. Fortunately, the culture is slowly changing. In computational condensed matter physics, the ALPS and Abinit projects provide open implementations of a variety of commonly used methods and algorithms [13] [14]. In the wider scientific community, IPython is a shining example of building a powerful computational tool collaboratively, with a huge impact across disciplines [15].

Our QCA exact diagonalization implementation is written in C++ and uses the excellent Eigen linear algebra library [16]. Matrices are stored in sparse representation, except for the block-wise diagonalization itself, performed by Eigen, where we use dense matrices. The basis states can be filtered and sorted, for example to truncate the Hilbert space to a specific charge sector and to exploit symmetries. We do not build the Hamiltonian matrix directly, but instead construct creation and annihilation operator matrices. Therefore, operators such as the Hamiltonian and the polarization can be expressed in an intuitive, almost mathematical notation. We employ the curiously recurring template pattern to achieve simple static polymorphism, avoiding the overhead of runtime polymorphism [17]. In less abstract terms, this allows us to reuse code, for example the Hamiltonian, for the conceptually similar, but physically quite different various QCA models which we are going to introduce in detail in the next chapter. Our C++ code cannot be executed directly, but is instead compiled as an extension module for the Python language, via the Boost library's Boost.Python [18]. We also use the unit testing framework from the Boost library. In our experience, making the C++ code available in Python provides enormous benefits. With Python data input, output and storage becomes a breeze, especially compared to the chore these tasks are in pure C++. Python makes it easy to script and distribute (i.e. simply parallelize) simulation runs, and, being well established in the scientific community, comes with extensive libraries for data analysis and plotting, for example SciPy and Matplotlib [19] [20]. Consequently, the integration with Python facilitates quickly trying out new ideas, implementing new features and more fluid data analysis. The advent of the fantastic IPython notebook ties all of these pieces together in a consistent, productive and highly enjoyable workflow [15]. The IPython notebook is also an apt format for effectively communicating results with colleagues. The disadvantages of the Python integration are the additional dependencies, although both Python and Boost are commonly available on any number of platforms these days, and the more involved (and hence error-prone) build process. We have written a small Python library to support our data storage and organization needs. The library facilitates storing and retrieving data in standard file formats

and allows to define and run "numerical experiments," which can be distributed across multiple computers. Both the QCA exact diagonalization code and the Python library are available under an open license on GitHub [21] [22].

Chapter 2

Approximations

2.1 Fixed charge model

Exact diagonalization scales exponentially with system size. With the full *grand canonical* QCA Hamiltonian (1.1) only devices of up to two cells are computationally feasible. Therefore, we need to introduce approximations to access larger systems. Approximating means to simplify. However, by carefully establishing successive approximations and their limits, we also reduce the problem to its essential ingredients and thus, hopefully, we gain a better understanding of the QCA approach. As a first step, we reduce the Hilbert space to states with a fixed number of particles per cell. We disallow any charge fluctuations, both for the system as a whole and for each individual cell. With that, we omit the chemical potential term in the Hamiltonian, $\mu = 0$, and prohibit inter-cell hopping. This is a major simplification. However, it is in line with the QCA idea: the approach requires a fixed number of charges per cell, typically two electrons, and cells are thought to interact only via Coulomb forces. If the *fixed charge* approximation is not valid for a given system, then there is no hope of implementing QCA on it. For experimental systems like the atomic silicon quantum dots, it should always be possible, at least in principle, to tune the system parameters so that for a given cell layout each cell is occupied by the same number of electrons. The two-electrons-per-cell sector has to be lowest in energy and other particle number sectors need to be sufficiently gapped out, that is, at an energy much larger than temperature. Of course, in practice there are very clear limits as to how much the system parameters can be tuned. Any QCA cell layout considered within the fixed charge approximation cannot necessarily be readily implemented on a given real-world material system.

For the fixed charge model, the state space scales as $N_s = \binom{8}{2}^{N_c} = 28^{N_c}$ (N_c is the number of cells). Using symmetries, the largest block of the Hamiltonian matrix is the spin zero sector, of size $N'_s = 16^{N_c}$. On conventional computer hardware, systems of up to four cells are possible, with memory requirements of 32GB. However, such calculations
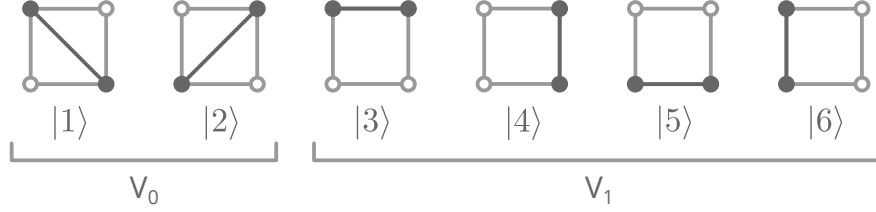
Figure 2.1: The six bonds of a QCA cell. The basis of a QCA cell in the fixed charge picture consists of six bonds and four doubly occupied dots. Each bond corresponds to one spin singlet and three spin triplet states. The bond model neglects doubly occupied states and keeps only one state per bond for a total of six states per cell. From those, the Ising approximation only retains the two lowest energy states, $|1\rangle$ and $|2\rangle$ with energy V_0.

take very long and therefore three-cell systems are the practical limit.

2.2 Bond model

At its heart, QCA is a semi-classical idea. It relies dominantly on charge-charge interactions and ignores the particle spin. Therefore, as a next step in our quest to access larger system sizes, we neglect the spin degrees of freedom. The 28 states of each cell in the fixed charge model can be reorganized into four doubly occupied dots and six bonds, illustrated in Fig. 2.1. Each bond corresponds to one spin singlet and three spin triplet states. The *bond* approximation only keeps one state for each bond and discards the doubly occupied states as well. With the bond model we thus assume that singlet and triplet states are qualitatively and energetically equivalent, and that doubly occupied dots are sufficiently gapped out, that is, $U \gg T$. Because QCA ignores the spin, singlets and triplets should be qualitatively the same—for example, they should yield the same cell polarizations. However, we can speculate that virtual double-occupancy lowers the energies of the singlet states and therefore introduces a small singlet-triplet splitting. Neglecting this small splitting presumably does not introduce a large error, but we will have to verify this assumption and look at the splitting in more detail in due course. For the bond model the QCA Hamiltonian reduces to

$$H = -\sum_{\langle ij \rangle} t c_i^\dagger c_j + \sum_{i<j} V_{ij} \left(n_i - q\right) \left(n_j - q\right) . \tag{2.1}$$

With six bond states per cell, the Hilbert space of the bond model is $N_s = 6^{N_c}$ (N_c the number of cells). Five and six cells are doable, with memory requirements of 460MB and 16GB, respectively, but for practical calculations five-cell systems really are the limit. For the bond model there are no symmetries that can be exploited.
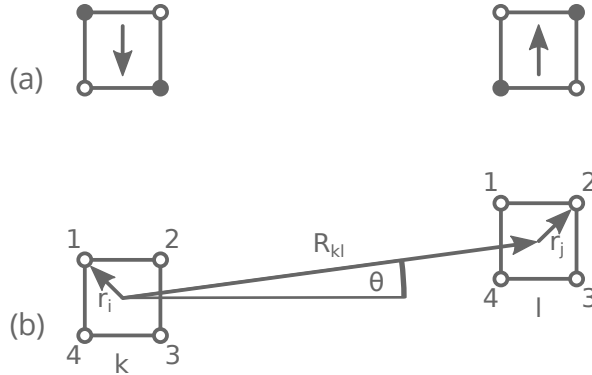
Figure 2.2: (a) The Ising approximation identifies each cell with a pseudo spin. Logic 0 corresponds to spin down and logic 1 to spin up. (b) QCA cells k and l.

2.3 Ising model

A linear array of QCA cells where each cell has a state of logic 0 or 1 is reminiscent of a 1D spin $\frac{1}{2}$ chain. Indeed, if we reduce the basis to only two states per cell, down from six states in the bond picture, we can map the QCA system to a transverse-field Ising model with long-ranged interactions. This is an attractive proposition: The smaller Hilbert space allows for larger system sizes with our exact diagonalization method; more importantly, the transverse-field Ising model is amenable to sign-problem-free Stochastic series expansion (SSE) quantum Monte Carlo schemes [23]. These methods do not scale exponentially[1] and consequently allow access to much larger systems. Last, but not least, such a mapping connects the QCA approach to the established and well studied Ising model. The prospect hinges on the assumption that the two-states-per-cell basis actually is a good approximation for QCA systems. And while bistable two-state cells are certainly the picture we have in mind when we talk about QCA, it is not *a priori* clear whether this is a correct physical picture. The transverse-field Ising model is equivalent to the two-states-per-cell approximation that has been used extensively, but was never satisfyingly derived, in the literature to study the dynamics of QCA systems.

We use the bond Hamiltonian (2.1) as the starting point. We had already discussed in the last chapter that such a Hamiltonian can be decomposed into single-cell terms and cell-cell interaction terms,

$$H = \sum_k H_k^c + \sum_{k<l} H_{kl}^{cc} . \tag{2.2}$$

---

[1]SSE quantum Monte Carlo methods roughly scale as $N \ln N$ where N is the system size.

In comparison, the transverse-field Ising model is described by

$$\tilde{H} = -\sum_k \gamma S_k^x + \sum_{k<l} J_{kl} S_k^z S_l^z \,. \tag{2.3}$$

Thus, we would like to map the single cell term H_k^c to the transverse-field term $-\gamma S_k^x$ and the Coulombic cell-cell interaction H_{kl}^{cc} to the Ising term $J_{kl} S_k^z S_l^z$. Each cell k is identified with a pseudo spin S_k^z, specifically logic 0 with spin down and logic 1 with spin up, as illustrated in Fig. 2.2(a). We will first look at how the QCA cell can be represented by only two basis states and derive an approximate expression for the transverse field γ. Then we will use a multipole expansion to derive J_{kl} from the cell-cell Coulomb interaction.

To arrive at a single-cell-basis with only two states we can, in principle, follow a similar prescription as for the fixed charge and bond approximations: we neglect high-energy states which are assumed to be gapped out. In this case, the neglected states are the four edge states with Coulomb energy V_1, $|\psi_Q\rangle = \{|3\rangle, |4\rangle, |5\rangle, |6\rangle\}$, illustrated in Fig. 2.1, where we have introduced $|\psi_Q\rangle$ to denote the high-energy subspace of the single-cell Hilbert space. We only keep the low-energy diagonal states $|\psi_P\rangle = \{|1\rangle, |2\rangle\}$ with Coulomb energy V_0. Of course, these two states are exactly our logic 0 and logic 1 state, or, in the Ising language, $|\downarrow\rangle \doteq |1\rangle$ and $|\uparrow\rangle \doteq |2\rangle$. Here, $|\psi_P\rangle$ denotes the low-energy subspace. For the high-energy states to be sufficiently gapped out, we require $\Delta V = V_1 - V_0 \gg T$. In contrast to the fixed charge and bond model, merely truncating the Hilbert space is not sufficient for the Ising model. For our previous two approximations, the Hamiltonian had remained essentially unchanged, apart from dropping no longer relevant terms, such as the chemical potential term or the Hubbard U term. The retained states were exactly the same states as in the full, untruncated model. But with only two states per cell the existing Hamiltonian (2.1) does not "work": There is no process that takes the cell from $|1\rangle$ to $|2\rangle$ and the system would be stuck in either of the two spin states eternally. In the bond picture, in comparison, for the system to transition from state $|1\rangle$ to $|2\rangle$ it can take different paths, for example $|1\rangle \rightarrow |3\rangle \rightarrow |2\rangle$, consisting of two hopping processes with an interim high-energy edge state. We need to derive an effective, low-energy Hamiltonian from the bond model that treats those processes perturbatively, as *virtual* excitations, yielding an effective hopping term for the transition $|1\rangle \leftrightarrow |2\rangle$. This effective hopping is precisely the transverse field γ which flips the spin in the Ising picture.

A single QCA cell is described by the time-independent Schrödinger equation $H_k^c |\psi\rangle = E_k |\psi\rangle$, with $|\psi\rangle = [|\psi_P\rangle |\psi_Q\rangle]$. Our aim it to truncate the basis to $|\psi_P\rangle$ and derive an effective Hamiltonian $\tilde{H}_k^c$ with the subspace Schrödinger equation $\tilde{H}_k^c |\psi_p\rangle = E_k |\psi_p\rangle$. Using the basis depicted in Fig. 2.1, the single-cell bond Hamiltonian is very simple and can be written down explicitly. As the single-cell Hamiltonian is the same for all cells, we can

drop the index k.

$$H^c = \left(\begin{array}{cc|cccc} V_0 & 0 & -t & -t & -t & -t \\ 0 & V_0 & -t & -t & -t & -t \\ \hline -t & -t & V_1 & 0 & 0 & 0 \\ -t & -t & 0 & V_1 & 0 & 0 \\ -t & -t & 0 & 0 & V_1 & 0 \\ -t & -t & 0 & 0 & 0 & V_1 \end{array} \right) \tag{2.4}$$

$$= \left(\begin{array}{cc} H_{PP} & H_{PQ} \\ H_{QP} & H_{QQ} \end{array} \right)$$

Here, we have partitioned the Hamiltonian into four blocks, H_{PP}, H_{QQ}, H_{PQ}, and H_{QP}, corresponding to the low-energy subspace $|\psi_P\rangle$, the high-energy subspace $|\psi_Q\rangle$, and transitioning between the subspaces. With this partitioned Hamiltonian the time-independent Schrödinger equation is

$$\begin{pmatrix} H_{PP} & H_{PQ} \\ H_{QP} & H_{QQ} \end{pmatrix} \begin{pmatrix} \psi_P \\ \psi_Q \end{pmatrix} = E \begin{pmatrix} \psi_P \\ \psi_Q \end{pmatrix} . \tag{2.5}$$

Writing out the matrix equation as two equations explicitly, and eliminating $|\psi_Q\rangle$ yields

$$H_{PP} |\psi_P\rangle + H_{PQ} \frac{1}{E - H_{QQ}} H_{QP} |\psi_P\rangle = E |\psi_P\rangle \tag{2.6}$$

and therefore

$$\tilde{H}^c = H_{PP} + H_{PQ} \frac{1}{E - H_{QQ}} H_{QP} . \tag{2.7}$$

Assuming that the system is predominantly in the subspace spanned by $|\psi_P\rangle$ and additionally that the hopping is very small, $t \ll V_0$, we can approximate $E \approx V_0$. We write out the matrix multiplications and use $(H_{PP})_{ij} = (V_0)_{ii} \delta_{ij}$, $(H_{PQ})_{ij} = (-t)_{ij}$, and so on. The effective Hamiltonian becomes

$$\begin{aligned} \tilde{H}^c_{ij} &= (V_0)_{ii} \delta_{ij} + (-t)_{ik} (V_0 - V_1)^{-1}_{kk} (-t)_{kj} \\ &= (V_0)_{ii} \delta_{ij} - \left(\frac{4t^2}{\Delta V} \right)_{ij} . \end{aligned} \tag{2.8}$$

As the system remains unchanged upon adding a constant term to the Hamiltonian, we can subtract the constant diagonal term $\tilde{H}_{ii} = V_0 - \frac{4t^2}{\Delta V}$, and arrive at

$$\tilde{H}^c = \begin{pmatrix} 0 & -\frac{4t^2}{\Delta V} \\ -\frac{4t^2}{\Delta V} & 0 \end{pmatrix} . \tag{2.9}$$

The off-diagonal matrix elements are the effective hopping, transitioning the system between its two states $|1\rangle \leftrightarrow |2\rangle$. If we now compare this matrix with the transverse-field term of the Ising model,

$$
\begin{aligned}
\tilde{H}^c &= -\gamma S_k^x \\
&= -\frac{1}{2}\gamma \left(S_k^+ + S_k^- \right) \\
&= \begin{pmatrix} 0 & -\frac{1}{2}\gamma \\ -\frac{1}{2}\gamma & 0 \end{pmatrix} ,
\end{aligned}
\tag{2.10}
$$

we identify the effective hopping as the transverse field γ,

$$
\gamma = \frac{8t^2}{\Delta V} .
\tag{2.11}
$$

The effective hopping is a virtual process involving two hopping processes in the original bond model, yielding the t^2 in the numerator, and an interim high-energy state gapped out by ΔV, hence the ΔV in the denominator. To arrive at the expression for the effective hopping γ we used the assumptions $\Delta V \gg T$ and $t \ll \Delta V$. As a reminder, $\Delta V = V_1 - V_0 = \frac{2-\sqrt{2}}{2}\frac{1}{a} \approx 0.3V_1$. Notably, the energy gap is independent of the compensation charge q. As the derivation used only a single cell, it is also implicitly assumed that the perturbations from other cells in the system are small, at least as far as the effective hopping is concerned. If the hopping depended on the state of nearby cells, then the effective Hamiltonian would be much more involved and certainly could not be mapped to an Ising-like model.

We have successfully derived an effective hopping term and therefore also an effective two-state model for the QCA Hamiltonian. With only two states per cell the Hilbert space scales as $N_s = 2^{N_c}$ (N_c the number of cells) and up to 14 cells are computationally feasible, with memory requirements of 2GB. In practice, we restrict the calculations to a maximum of 12 cells. For our calculations, we can use the two-state approximation with the effective hopping term, but still retain the original cell-cell interaction term H_{kl}^{cc}. From a computational point of view, nothing is gained by expressing the cell-cell interaction as an Ising interaction. However, deriving J_{kl} from H_{kl}^{cc} is very rewarding conceptually and will already allow some key insights into the characteristics of QCA devices. Therefore, we now undertake the derivation of an expression for J_{kl}. The obvious starting point is the

cell-cell interaction term H_{kl}^{cc},

$$H_{kl}^{cc} = \sum_{\substack{i\in k \\ j\in l}} V_{ij}\,(n_i - q)\,(n_j - q)$$

$$H_{kl}^{cc} = \sum_{\substack{i\in k \\ j\in l}} \frac{(n_i - q)\,(n_j - q)}{|\boldsymbol{R}_{kl} + \boldsymbol{r}_j - \boldsymbol{r}_i|} \tag{2.12}$$

$$= \sum_{\substack{i\in k \\ j\in l}} \frac{n_i n_j - q(n_i + n_j)}{|\boldsymbol{R}_{kl} + \boldsymbol{r}_{ij}|}\,,$$

where i and j sum over the four dots $1\ldots 4$ of cell k and l, respectively, and $\boldsymbol{R}_{kl}$ denotes the vector between the centres of the cells, see Fig. 2.2(b). We have introduced $\boldsymbol{r}_{ij} = \boldsymbol{r}_j - \boldsymbol{r}_i$ and dropped the constant q^2 term. There are only four possible configurations for two interacting cells: $\uparrow\uparrow$, $\downarrow\downarrow$, $\uparrow\downarrow$, and $\downarrow\uparrow$. Using the shorthand notations $V_{ij} = \frac{1}{|\boldsymbol{R}_{kl}+\boldsymbol{r}_{ij}|} + \frac{1}{|\boldsymbol{R}_{kl}-\boldsymbol{r}_{ij}|}$ and $V_{00} = \frac{1}{|\boldsymbol{R}_{kl}|}$, we calculate their energies explicitly.

$$E^{\uparrow\uparrow} = (1 - 2q)\,(2V_{00} + V_{24}) - q\,(2V_{12} + 2V_{14}) \tag{2.13}$$

$$E^{\downarrow\downarrow} = (1 - 2q)\,(2V_{00} + V_{13}) - q\,(2V_{12} + 2V_{14}) \tag{2.14}$$

$$E^{\uparrow\downarrow} = (1 - 2q)\,(V_{12} + V_{14}) - q\,(4V_{00} + V_{13} + V_{24}) \tag{2.15}$$

$$E^{\downarrow\uparrow} = (1 - 2q)\,(V_{12} + V_{14}) - q\,(4V_{00} + V_{13} + V_{24}) \tag{2.16}$$

Note that the expression for two spin-down cells can be obtained from the expression for two spin-up cells (and similarly $E^{\uparrow\downarrow}$ from $E^{\downarrow\uparrow}$) simply by rotating the system by $90°$, or equivalently, by permuting the dot numbering: $1, 2, 3, 4 \rightarrow 4, 1, 2, 3$. Symmetries can be exploited, for example $V_{43} = V_{12}$. Evidently, $E^{\uparrow\downarrow} = E^{\downarrow\uparrow}$, which, given the highly symmetric geometry of those cell arrangements, does not come as a surprise. But crucially, we find $E^{\uparrow\uparrow} \neq E^{\downarrow\downarrow}$. Therefore, we have a system with three distinct energy levels which we cannot hope to represent with the solely two-level Ising term $J_{kl}S_l^z S_l^z$. Instead, let us try to map to a *modified* Ising model with a three-level cell-cell interaction term of the form

$$\tilde{H}_{kl}^{cc} = J_{kl}S_k^z S_l^z + J'_{kl}\,(S_k^z + S_l^z)\,. \tag{2.17}$$

For this Hamiltonian we have the energies

$$\tilde{E}^{\uparrow\uparrow} - \tilde{E}^{\uparrow\downarrow} = 2J_{kl} + 2J'_{kl} \tag{2.18}$$

$$\tilde{E}^{\downarrow\downarrow} - \tilde{E}^{\uparrow\downarrow} = 2J_{kl} - 2J'_{kl} \tag{2.19}$$

which yields

$$J_{kl} = \frac{1}{4}\left(\tilde{E}^{\uparrow\uparrow} + \tilde{E}^{\downarrow\downarrow} - 2\tilde{E}^{\uparrow\downarrow}\right) \tag{2.20}$$

$$J'_{kl} = \frac{1}{4}\left(\tilde{E}^{\uparrow\uparrow} - \tilde{E}^{\downarrow\downarrow}\right)\,, \tag{2.21}$$

and therefore, identifying $E^{\uparrow\uparrow} = \tilde{E}^{\uparrow\uparrow}, E^{\downarrow\downarrow} = \tilde{E}^{\downarrow\downarrow}$, and so on,

$$J_{kl} = \frac{1}{4} \left(4V_{00} + V_{13} + V_{24} - 2V_{12} - 2V_{14} \right) \tag{2.22}$$

$$J'_{kl} = \frac{1}{4} \left(1 - 2q \right) \left(V_{24} - V_{13} \right) . \tag{2.23}$$

These results, while abstract, are remarkable in two ways. First, the newly introduced term J'_{kl} vanished for $q = \frac{1}{2}$. In this case, $E^{\uparrow\uparrow} = E^{\downarrow\downarrow}$. Thus, for charge neutral cells we recover the genuine, unmodified transverse-field Ising model. Second, the Ising J_{kl} itself is independent of the compensation charge q. We will see that J_{kl} is the quadrupole-quadrupole cell-cell interaction, to leading order. Thus, it is fair to say that J_{kl} is the pure QCA interaction. With the above equations we can also already look at rotational symmetries of J_{kl} and J'_{kl}: J_{kl} is invariant under rotations by $90°$ as can be seen by permuting the dots $1, 2, 3, 4 \rightarrow 4, 1, 2, 3$. This is what we expect intuitively. For example, a horizontal straight line of cells ($\theta = 0°$) should behave exactly the same as a vertical straight line of cells ($\theta = 90°$). In contrast, J'_{kl} is not invariant under rotations by $90°$. In fact, applying the same dot permutation yields $J'_{kl} \xrightarrow{90°} -J'_{kl}$. Consequently, J'_{kl} is symmetric under rotations by $180°$. It is also clear that a non-zero J'_{kl} breaks the system's symmetry under spin rotation—$\tilde{H}^{cc}_{kl}$ is not unchanged for $\uparrow\uparrow \rightarrow \downarrow\downarrow$. This has profound implications for QCA. For non-zero J'_{kl} we would, for example, expect different polarization responses for two spin-down cells versus two spin-up cells, and as a consequence the device would behave differently for logic 0 and logic 1 signals. From an application point of view, this is definitely not what we want. For QCA operation we therefore require charge neutral cells and a genuine, unmodified Ising model.

To obtain more tangible expressions for J_{kl} and J'_{kl} we do a multipole expansion of the V_{ij} terms. Specifically,

$$\frac{1}{|\boldsymbol{R}_{kl} \pm r_{ij}|} = \frac{1}{R_{kl}} \left(1 \pm 2 \frac{\boldsymbol{r}_{ij}\hat{\boldsymbol{R}}_{kl}}{R_{kl}} + \frac{r_{ij}^2}{R_{kl}^2} \right)^{-1/2}$$
$$= \frac{1}{R_{kl}} \left(1 \pm x + y \right)^{-1/2} \tag{2.24}$$

is Taylor-expanded in x and y, keeping all terms up to $\mathcal{O}\left(\frac{a^4}{R_{kl}^5} \right)$, which corresponds to quadrupole-quadrupole interactions. Plugging the results of the expansion back into Eqs. (2.22) and (2.23) yields

$$J_{kl} = \frac{1}{32} \left(9 - 105 \cos 4\theta \right) \frac{a^4}{R_{kl}^5} \tag{2.25}$$

$$J'_{kl} = \left(1 - 2q \right) \left(\frac{3}{2} \sin 2\theta \frac{a^2}{R_{kl}^3} + \frac{5}{4} \sin 2\theta \frac{a^4}{R_{kl}^5} \right) . \tag{2.26}$$

The leading order term of J_{kl} is R^{-5}, the quadrupole-quadrupole interaction. In contrast, the leading order term of J'_{kl} is R^{-3} and therefore, in general, J'_{kl} would be the dominating term—yet another argument why a non-zero J'_{kl} is highly undesirable for functioning QCA devices. Of course, we find our general symmetry observations confirmed by these more concrete expressions for J_{kl} and J'_{kl}: the former is invariant under $90°$ rotations, the latter only under rotations of $180°$. Both terms vanish at select angles. For example, we have $J'_{kl} = 0$ for $\theta = 0°$, so that at least for an exactly straight line of cells we recover the unmodified Ising model, even for non-charge-neutral cells. This does not help when building more complex devices than a wire, of course, but might still be useful for some experiments. As another example, $J_{kl} = 0$ for $\theta = 22.5°$. Conceivably, this could be exploited for device applications, to decouple closely spaced cells. As multipole expansions, the obtained expressions for J_{kl} and J'_{kl} should be valid for large cell-cell distances. In principle, an arbitrary number of higher order terms can be included to make the expressions as exact as desired. In practice on the computer, however, we do not use the multipole expansion at all, but simply sum up all Coulomb interactions exactly. We will see in due course that for the small cell-cell distances that we are typically interested in, an expansion up to R^{-5} is indeed not sufficient, and higher order terms would have to be included.

In summary, we have successfully mapped the QCA bond Hamiltonian (2.1) to a modified transverse-field Ising model,

$$\tilde{H} = -\sum_k \gamma S_k^x + \sum_{k<l} \left[J_{kl} S_k^z S_l^z + J'_{kl} \left(S_k^z + S_l^z \right) \right] , \tag{2.27}$$

where J_{kl} and J'_{kl} are given by Eqs. (2.25) and (2.26), and γ by Eq. (2.11).

2.4 Validity of the approximations

In the last three sections we have introduced three successive approximations for the QCA Hamiltonian: the fixed charge model, the bond model, and the Ising model. However, even though we know the theoretical limits in which those approximations become exact, we have given little thought to the practical limits. Numerical benchmarks will help us establish the parameter regimes where we can use the approximations and get sufficiently accurate results, and also give us a better understanding of how the approximations behave in those parameter ranges.

The fixed charge approximation is a Hilbert space truncation where we only keep the states with exactly two electrons per cell. Fig. 2.3(a) compares the density of states of the fixed charge model against the exact grand canonical model for a two-cell system. The chemical potential is $\mu = 250$ and the nearest-neighbour Coulomb energy is $V_1 = 100$, whereas the on-site Coulomb repulsion is $U = 1000$. The energies are in units of the hopping t, with $t = 1$. The cells are placed a distance $d/a = 3$ apart, horizontally. This system does not have any compensation charges, hence $q = 0$. The approximation reproduces the
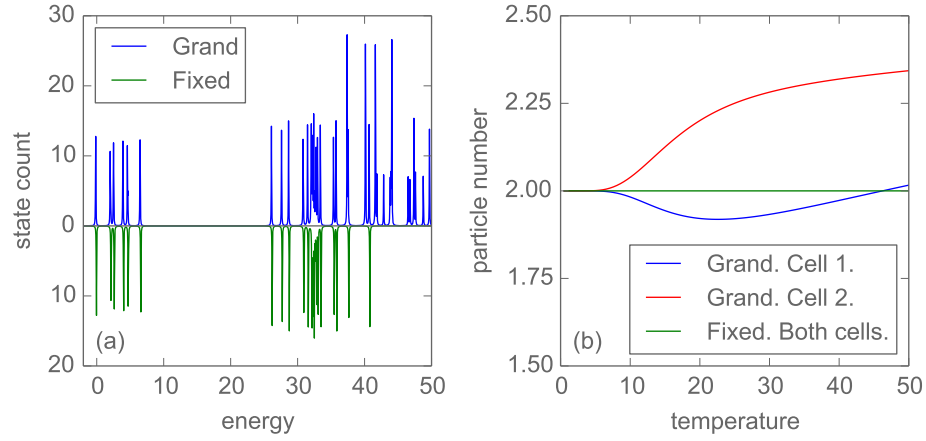
Figure 2.3: (a) Low-energy density of states of the exact grand canonical and the approximative fixed charge two-cell QCA system. For small energies the curves agree perfectly (up to $E \lesssim 35$). (b) Particle number per cell over temperature for the same two-cell system. The curves diverge for $T \gtrsim 10$.
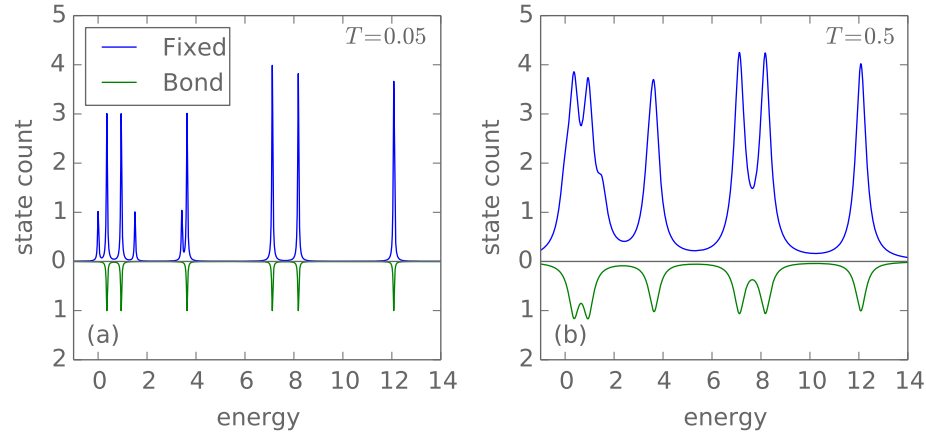

Figure 2.4: (a) Low-energy density of states of a one-cell QCA system for both the fixed charge and the bond model. The bond approximation only reproduces the triplet states, but omits the singlet states. The "measurement" temperature is indicated. (b) The same spectrum, but "measured" at a higher temperature. The singlet-triplet splitting is "washed out" at large enough temperatures: the singlet and triplet peaks are no longer separately resolved and each bond model state corresponds to four fixed charge states at roughly the same energy.

low-energy spectrum exactly, in the plot up to $E \lesssim 35$. Therefore, as long as the two-electrons-per-cell sector is lowest in energy and the temperature is small compared to the energy of the next charge sector, the model works perfectly. Fig. 2.3(b) plots the number of particles per cell over temperature and demonstrates the breakdown of the approximation. Whereas the fixed charge model gives, per definition, a constant number of particles over the whole temperature range, the grand canonical system's cell occupancies start to diverge from two electron per cell at around $T \sim 10$. This roughly corresponds to the energy states the fixed charge model misses at $E \gtrsim 35$. A small deviation from exactly two electrons per cell is not detrimental to QCA, a cell occupied by only one or by three electrons, however, renders QCA non-functional. We often use the fixed charge model as the starting point and assume, without further investigation, that a practical QCA implementation can be tuned to be in the right charge regime at a given temperature.

The bond model neglects doubly occupied states and represents the four states of a bond—one singlet and three triplets—with only one single bond state. The model thus assumes that singlet and triplet states are energetically equivalent, but we had already asserted that we might expect a small singlet-triplet splitting. Fig. 2.4(a) shows the density of states of a single QCA cell for both the fixed charge and the bond model. The hopping is again $t = 1$, the nearest-neighbour Coulomb energy is $V_1 = 20$, and the on-site Coulomb repulsion is $U = 10^6$—practically at infinity. A driver cell placed at a distance $d/a = 3$ to the left of the single cell sets an input. We have chosen the driver cell's polarization to be $P_D = 1$. Indeed, each bond state corresponds to three fixed charge states—the triplet—and one "close-by" state—the singlet. They are not energetically equivalent, but split by a small energy gap, ΔE_S, the singlet-triplet splitting. Like the fixed charge model, the bond approximation truncates the Hilbert space and the retained states are exact. Evidently, the bond model keeps one triplet state, but discards the other two and the singlet. We speculate that, similar to the antiferromagnetic Heisenberg coupling constant J emerging in the low-energy limit of the Hubbard model (with $J \sim \frac{t^2}{U}$) [24], here, virtual excitations to high-energy doubly occupied states lower the energy of the singlet state and make it the ground state. Because the bond model misses those doubly occupied states, it cannot accommodate singlet states and hence reproduces the triplet states. Consequently, we cannot hope that the bond model is correct for ground state and low-temperature properties. We assert that as long as the singlet-triplet splitting is "washed out", that is, as long as the temperature is much larger than the singlet-triplet gap, $T \gg \Delta E_S$, the approximation should give good results. At high enough temperatures, the system no longer "sees" the difference between the singlet and the triplet states. This is illustrated in Fig. 2.4(b) where the spectrum is "measured" at a higher temperature:[2] the singlet and triplets are no longer resolved separately. Instead, each bond state corresponds to four

---

[2] We calculate the density of states graphs by folding the energy eigenvalues of the system—a delta function energy spectrum—with a Lorentzian with the half-width at half-maximum set by a "measurement" temperature. Very roughly speaking, this corresponds to a photoemission / inverse photoemission spectroscopy experiment at this temperature.

fixed charge states at roughly the same energy.

The figure shows all six bond states of the single cell—the complete spectrum apart from the doubly occupied states. As this cell is perturbed by a nearby driver cell with $P_D = 1$, the ground state is qualitatively closest to the logic 1 state, or $|2\rangle$ in Fig. 2.1. Similarly, the first excited state is similar to $|1\rangle$, or logic 0, and the four higher energy states correspond to $|4\rangle$, $|5\rangle$, $|3\rangle$, and $|6\rangle$, in that order. Of course, in general the energy eigenstates are a mixture of all basis states, but we can still characterize them by the most dominantly contributing basis state. As this is a non-charge-neutral system, $q = 0$, with a relatively small cell-cell distance $d/a = 3$, charge buildup tends to push the electrons to the far edge of the cell, thus making $|4\rangle$ lower in energy than $|6\rangle$.

Since the bond model ignores the singlet-triplet splitting, it is important to understand how the gap ΔE_S depends on various system parameters. To that end we picked out a few selected singlet-triplet states from the spectrum in Fig. 2.4(a) as examples. Contrary to expectations, for those states the gap ΔE_S did not change significantly with the on-site Coulomb repulsion U. However, it did become smaller for shorter and shorter cell-cell distances d. Most importantly, for the nearest-neighbour Coulomb energy V_1 we found $\Delta E_S \sim \frac{1}{V_1^p}$. The exponent is $p \sim 3$ when the cell "sees" a biasing external potential (e.g. $P_D = \pm 1$) and $p \sim 1$ otherwise (e.g. $P_D = 0$). Even though our method is anything but rigorous and the obtained results very likely not universally true, the findings should nonetheless give a good enough idea of the principal trends. Quite generally, the higher the overall Coulomb potential—large V_1 and small d—the smaller the singlet-triplet splitting and, conceivably, the more accurate the bond approximation. The bond model should work as long as $T \gg T_{min}$ with $T_{min} \sim \Delta E_S$, and as a very rough guideline we can use $\Delta E_S \sim \frac{t^2}{V_1}$. Of course, we also need $T \ll T_{max}$ with $T_{max} \sim U$, so that the doubly occupied states are gapped out.

To illustrate the limitations of the bond approximation we now look at a two-cell system: a horizontal line of cells with two active cells and a driver cell to the left. Fig. 2.5 shows the spectra and output polarizations of the system for two different Coulomb energies, $V_1 = 20$ and $V_1 = 100$. Otherwise the parameters are the same as for the one-cell system in the previous graph. In particular, the spectrum in Fig. 2.5(a) is exactly the same as in Fig.2.4(a), except that we have added one more cell to the system. Each bond state now corresponds to 16 ($4 \cdot 4$) fixed charge states. Looking at the four lowest-energy peaks in the spectrum, we see that the bond model exactly reproduces the nine triplet-triplet states, but misses the three singlet-triplet and the three triplet-singlet states (in the graph the corresponding two peaks are hardly distinguishable), as well as the single singlet-singlet ground state. The four lowest bond states should roughly correspond to, in that order, both cells being aligned with the driver cell (the ground state), only one of the two cells being aligned with the driver cell, and both cells being anti-aligned with the driver cell. Higher energy states have at least one of the cells not in the preferred diagonal states, $|1\rangle$ and $|2\rangle$, with electrons occupying predominantly the edge of a cell.
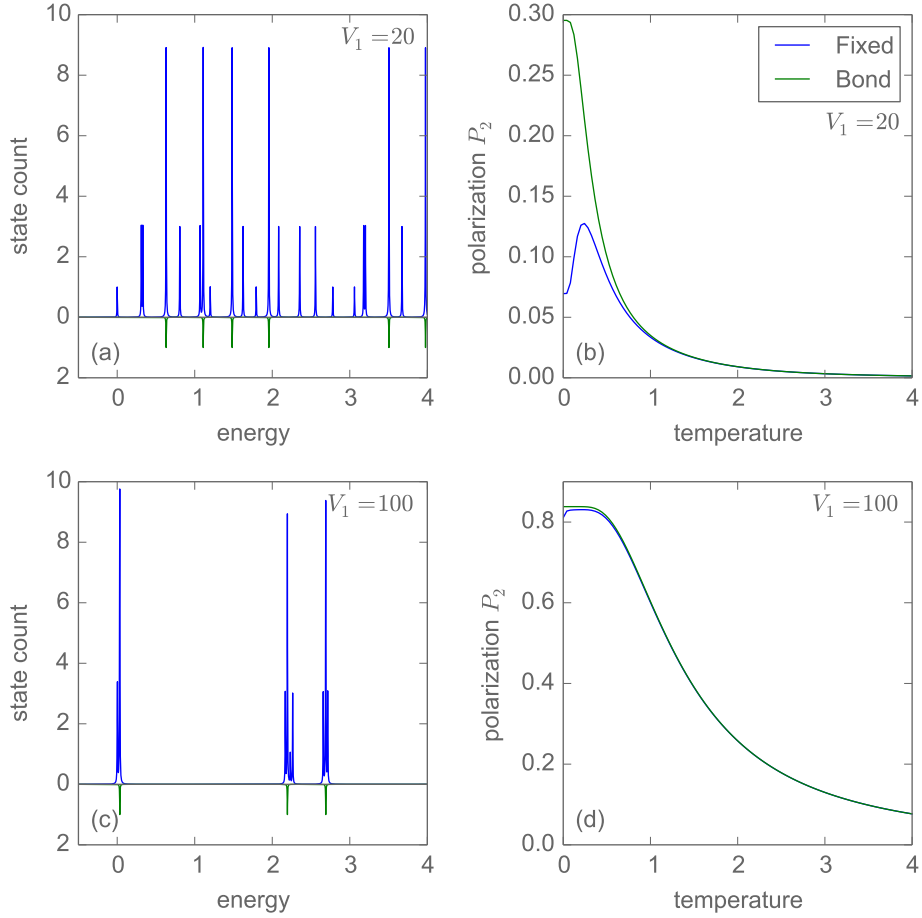
Figure 2.5: The two-cell fixed charge and bond systems at $V_1 = 20$ and $V_1 = 100$. (a)(c) Low-energy density of states. (b)(d) Output polarization P_2 over temperature. For a small Coulomb repulsion the density of states curves look qualitatively very different (a) and the bond approximation does not work very well (b). At a larger Coulomb repulsion the density of states curves look much more alike (c) and the bond approximation works much better (d).

Arguably, the spectra of the fixed charge and the bond model in Fig. 2.5(a) do not look very similar. Consequently, the polarization curves in Fig. 2.5(b) do not agree, especially at low temperatures. In fact, it is rather remarkable that given the widely dissimilar spectra, the polarizations actually do agree relatively well at higher temperatures, $T \gtrsim 1$. The bond model only reproduces the most populous energy states of the exact spectrum. Apparently, that is enough to give (almost) correct results at high temperatures. The lower the temperature, the more important become the few lowest lying energy states which the bond model misses. Very roughly speaking, the temperature where the bond model's polarization becomes accurate also matches the temperature where we saw the singlet-triplet splitting being washed out in Fig. 2.4(b). For the much larger Coulomb energy $V_1 = 100$ the spectra look much more alike, qualitatively, even though the bond model obviously still does not resolve all the lines of the exact density of states, as illustrated in Fig. 2.5(c). Therefore, the approximation works much better: the polarization curves agree down to much lower temperatures and even the discrepancy of the ground state polarizations is much reduced, as demonstrated in Fig. 2.5(d). Compared to the $V_1 = 20$ system, the ground state polarization is much larger and, generally, the larger the cell polarization, the better the agreement between bond and fixed charge model. We also note that in the spectrum the peaks are much more spaced out and thus the $V_1 = 100$ wire retains larger cell polarizations up to much higher temperatures. For any conventional material, a Coulomb energy scale such as we have chosen here, $V_1/t \geq 20$, where we have, of course, $U/t \gg V_1/t$, seems like an extremely large value. However, we will find that such Coulomb energies are generally in agreement with what the QCA approach itself requires, and we will discuss this in detail in the next chapter.

The polarization of the fixed charge model shows a curious bump at low temperatures, for example in Fig. 2.5(b), and similarly, if less visibly, in Fig. 2.5(d). Apparently, the ground state is not the most polarized state. Maximum polarization is reached at a small, but finite temperature. At the same time, for the bond model the ground state is the most polarized state and generally its zero-temperature polarization is larger than that of the fixed charge model. Interestingly, in contrast to the fixed charge model the bond model's ground state polarization is largely independent of the magnitude of the driver polarization and also only weakly influenced by the cell-cell distance d, especially for charge-neutral cells where no charge buildup occurs. Instead, it is predominantly set by V_1, and thus by V_1/t and the energy gap $\Delta V = V_1 - V_0$. Without an external perturbation such as a non-zero driver polarization the ground state polarization is zero, of course. But any infinitesimal external perturbation will instantly see the bond model's ground state become almost fully polarized. We interpret this behaviour as the ground state actually consisting of two energetically degenerate states, corresponding to $\pm P_{gs}$, where P_{gs} is the full ground state polarization for a given V_1. The smallest perturbation lifts this degeneracy and sees the system snapping to either $+P_{gs}$ or $-P_{gs}$. Now the bond model's ground state corresponds to the fixed charge model's triplet state—one of the lower lying excited states, but not the ground state. The true ground state of the more exact model is a single singlet state,
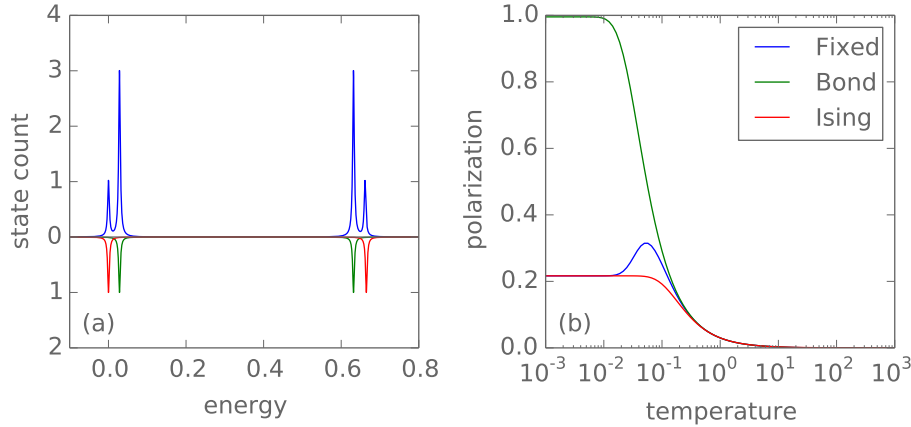
Figure 2.6: Comparing the fixed charge, bond, and Ising model for the one-cell charge-neutral QCA system. (a) Low-energy density of states. The Ising model reproduces the singlet and not the triplet states, as the bond model does. (b) Cell polarization over temperature. At larger temperatures $T \gtrsim 0.3$ all three models seem to agree. At $T = 0$ the bond model is wrongly fully polarized, whereas the Ising model exactly reproduces the fixed charge model's ground state polarization.

a superposition of the $+P_{gs}$ and $-P_{gs}$ (and other) states. Therefore, the polarization of the true ground state is generally smaller in magnitude than the polarization of the corresponding two triplet states, explaining the low temperature bump in the polarization curve and the larger polarization of the bond model's ground state.

The Ising approximation is derived as an effective low-energy model from the bond Hamiltonian. It is therefore qualitatively different from the previous two approximations: it is not merely a Hilbert space truncation. While the Ising model should resemble the bond model in the limit where the approximations in its derivation become exact, for less than optimal parameters the models' states need not be in perfect agreement. The derivation assumed $E \approx V_0$ (E the energy of the whole system) and therefore $t \ll \Delta V$ as well as $T \ll \Delta V$. Additionally, cells were assumed to be isolated, so the Ising model presumably requires reasonably large cell-cell distances. Naturally, the model inherits the limits of the bond approximation, and we would therefore expect $T \gg \Delta E_S$ (ΔE_S the singlet-triplet splitting) and $T \ll U$ as further requirements. It is important to keep in mind that the Ising model is not a low-energy model for the more exact fixed charge Hamiltonian—it is derived as the low-energy limit of the bond model, which, however, is not an accurate low-energy description of the fixed charge system. The approximation can also not hope to capture non-charge-neutral systems correctly. It simply lacks the edge states that are the manifestation of charge buildup, as discussed in the example of the one-cell bond system

above. We had seen in the derivation of the Ising model that non-charge-neutral cells are
very problematic for the QCA approach in general. Consequently, we will concentrate on
charge-neutral systems with a compensation charge $q = \frac{1}{2}$ for the remainder of the chapter.

To understand how the Ising approximation behaves, we again start by looking at
the density of states of a one-cell system, shown in Fig. 2.6(a). We have plotted both
the fixed charge and bond model's density of states for comparison and now use slightly
different system parameters: the nearest-neighbour Coulomb energy is $V_1 = 100$, the cell-
cell distance is $d/a = 4$, and the driver cell is only slightly polarized with $P_D = 0.1$. As
always, the hopping is $t = 1$. We are in for a surprise! Evidently, the Ising model reproduces
the singlet states and not the bond model's triplet states. In line with this observation,
the Ising model exactly matches the fixed charge model's ground state polarization, but
misses the triplet-bump at $T \sim 0.05$, as can be seen in Fig. 2.6(b). Here, for the charge-
neutral system, the bond model's ground state is fully polarized even at this large cell-cell
distance and for a very weak driver cell polarization. Even though we had derived the
Ising model from the bond Hamiltonian, it does not resemble the bond model at all, which
is very confusing. To lift the confusion, we first note that, even though the Ising model
correctly captures the fixed charge ground state of the single-cell system, this is not true
in general for larger systems, as we will see in a moment. Second, we need to be very
careful when we talk about the bond model. The bond Hamiltonian is simply a spinless
model that does not distinguish between singlet and triplet states. In contrast, the bond
model uses a concrete basis and we saw that it chooses the triplet states. Therefore, the
bond Hamiltonian, from which we derived the Ising model, and the bond model are not
equivalent. Because the Ising model is an effective low-energy model, it makes sense that
it captures the singlet states, which are lowest in energy. The Ising and bond states should
still eventually become energetically and qualitatively equivalent, in the limit where the
Ising model becomes exact and the singlet-triplet splitting goes to zero. On second thought,
the fact that the Ising model exactly reproduces the ground state of the one-cell system is
maybe not as surprising, because we had derived it precisely for a single, isolated cell.

Close inspection of the Ising model's only two states as compared to the equivalent fixed
charge model's states show that they are not exactly the same energetically. The difference
is hardly discernible in the plotted spectrum, but more pronounced for differently chosen
system parameters. Given that the Ising approximation is an effective model and used
several assumptions in its derivation, this is hardly surprising. For the single-cell system we
can easily study the error of the energies of the Ising states with respect to the fixed charge
states: the states are in better agreement for larger V_1 and smaller t. The error explodes
for very small cell-cell distances $d/a < 2$—when the assumption of isolated cells breaks
down—but is largely independent of d/a otherwise. Therefore, we find the assumptions
and limits of the derivation confirmed.

To be able to better quantitatively compare different models we introduce the relative

error of the polarization, defined as

$$\epsilon_k^I = \frac{\left| P_k^F - P_k^I \right|}{P_k^F} \tag{2.28}$$

for the Ising model. We use the fixed charge model as the reference. Hence, P_k^F refers to the polarization of cell k with the fixed charge model and P_k^I is the same polarization, but determined using the Ising model. The relative error for the bond model, ϵ_k^B, is defined equivalently. The relative error is independent of the magnitude of the polarization and therefore suitable for comparing models over wide parameter ranges. For best results it is also desirable to not drive the systems into full polarization. Once cells are saturated at $|P_k| \sim 1$ the quantitative differences between the models disappear. This is why for our calculations with the Ising model here, which generally require larger V_1/t ratios, we have chosen larger cell-cell distances and smaller driver cell polarizations, resulting in less polarized cells.

Fig. 2.7 shows the relative error over temperature together with the density of states for all three models for a two-cell system at $V_1 = 100$ and $V_1 = 200$. As before, we find that the bond approximation works much better when its spectrum looks qualitatively more similar to the fixed charge spectrum. At $V_1 = 100$ the bond model yields an almost fully polarized ground state, whereas the fixed charge model's zero-temperature polarization is much smaller, resulting in a very large relative error, as indicated in Fig. 2.7(b). At $V_1 = 200$, both the fixed charge and the bond system are almost fully polarized at low temperatures and the relative error is therefore very small, as demonstrated in Fig. 2.7(d). For these calculations we used $U = 1000$ for the on-site Coulomb repulsion, but otherwise the same parameters as for the one-cell system above. Accordingly, we can see that the bond model starts to diverge for $T \gtrsim 200$. Even at $T = 1000$ the error is relatively small, because the polarization is quite insensitive to doubly occupied dots, being defined solely as the difference in charge of one diagonal versus the other diagonal of the cell. Note that at these large temperatures the actual polarization is already very small.

Looking at the relative error of the Ising model, we first notice that it becomes very large for $T > T_{max}$ with $T_{max} \sim 5 \ldots 10$. Of course, this is a consequence of the Ising model missing the gapped out edge states, where the gap is $\Delta V \sim 0.3V_1$. Accordingly, T_{max} is larger for $V_1 = 200$ than for $V_1 = 100$, though maybe not by as much as we might expect. In stark contrast to the one-cell system, for two cells the Ising model's ground state no longer agrees with the ground state of the fixed charge model. The Ising zero-temperature polarization is generally smaller than the polarization of the more exact model, and, similarly to the bond model, the zero-temperature relative error decreases for increasing V_1. The relative error curves of the Ising model reveal that the temperature range where the error is actually small—that is, where the Ising model can be considered valid—is quite narrow. For $V_1 = 100$ it is almost like a sweet spot, a very narrow window around $T \sim 1$. For $V_1 = 200$ the situation is much better, the error is close to zero in the
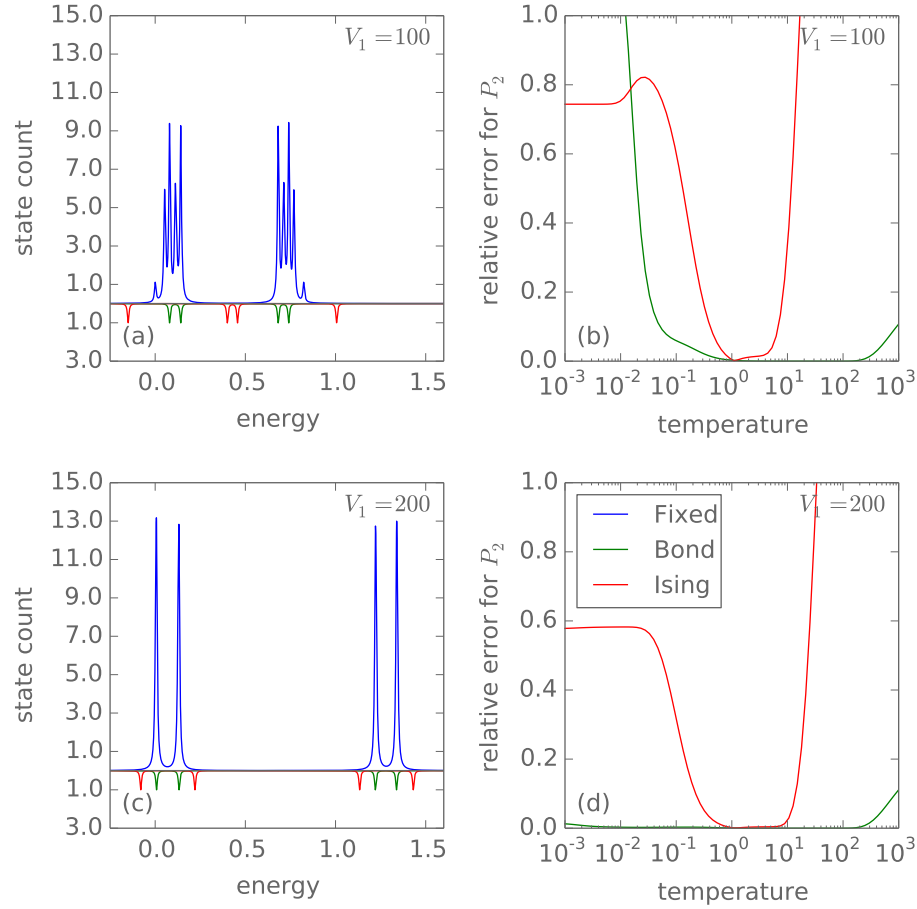
Figure 2.7: Comparing the fixed charge, bond, and Ising model for the two-cell charge-neutral QCA system at $V_1 = 100$ and $V_1 = 200$. (a)(c) Low-energy density of states. The Ising model's spectrum is qualitatively quite wrong, although it is in better agreement with the bond model's spectrum for larger V_1. (b)(d) Relative error of the output polarization of the bond and Ising model, with respect to the fixed charge model. The bond model's error is small over a large range of temperatures. At $T \sim U \sim 1000$ the neglected doubly occupied states become noticeable. The Ising model's error is small only over a relatively narrow temperature range. Its ground state no longer agrees with the fixed charge model's ground state.

temperature range $T = T_{min} \dots T_{max} \sim 0.8 \dots 8$. This temperature range only very weakly depends on the cell-cell distance d/a or the driver polarization P_D. It is dominantly set by V_1. Roughly speaking, the lower temperature limit T_{min} is set by the singlet-triplet splitting, which becomes smaller with increasing V_1, and the upper temperature limit T_{max} is set by ΔV which is, of course, directly proportional to V_1. Here we have, as always, kept the hopping constant at $t = 1$. In agreement with our analysis for the one-cell system, the relative error at a fixed temperature decreases with increasing V_1, but is largely independent of d/a as long as d/a is not too small.

The spectrum of the Ising approximation does not compare well with the fixed charge or bond model, especially at $V_1 = 100$, shown in Fig. 2.7(a). Clearly, the Ising model gets the energy levels completely wrong. However, we have to keep in mind that, in contrast to the bond model, the Ising model's states may be qualitatively different from the more exact models' states. Therefore, even though the spectrum looks completely wrong, the Ising model still does work correctly, if in a very small temperature range. In the right limit the Ising model should eventually resemble the bond model and accordingly, at $V_1 = 200$, the two models' spectra do look more agreeable, as can be seen in Fig. 2.7(c). The qualitative agreement of the spectra becomes better for smaller cell-cell distances and larger driver cell polarizations as well, thus generally when the cells are more fully polarized.

All told, the Ising model is a tricky approximation. It is conceptually confusing, because, even though it is derived from the bond Hamiltonian, it does not exactly resemble the bond model. Adding to this confusion is the fact that it gets the ground state of the one-cell fixed charge system right. From a practical point of view, the Ising model requires very large V_1/t ratios and its operational window can be very small, unless one is willing to go to obscenely large V_1/t ratios. Therefore, for moderately large Coulomb energies, great care should be exercised when using the Ising approximation. Calculations should be verified with a more exact model as much as possible and the error, and trends of the error, should be kept in check. Where an explicit verification is not possible, for larger systems, its results should be taken with a grain of salt.

As a final step, we look at a few concrete systems and their error trends. For a horizontal wire with three to five cells, a cell-cell distance of $d/a = 4$, and a nearest-neighbour Coulomb energy $V_1 = 100$, Fig. 2.8(a) shows the relative error as a function of the number of cells in the system. For these larger systems the Ising approximation and its error are benchmarked against the bond model and not the fixed charge model as before. We notice that for these wires the error is quite a bit smaller at $T = 2$ compared to $T = 1$, and an error of 1% seems to be the best we can do. Most worryingly, the error increases with the number of cells in the wire. This trend holds quite generally, for a range of systems with different cell-cell distances d/a and Coulomb energies V_1. Consequently, we expect the error to grow with increasing system sizes and once the systems are too large for bond model calculations, we will not be able to give a good upper error bound. The error will become uncontrolled. On a slightly more optimistic note, the error seems to decrease from cell to cell inside each wire. This is explored in more detail in Fig. 2.8(b), where we have plotted the error of each
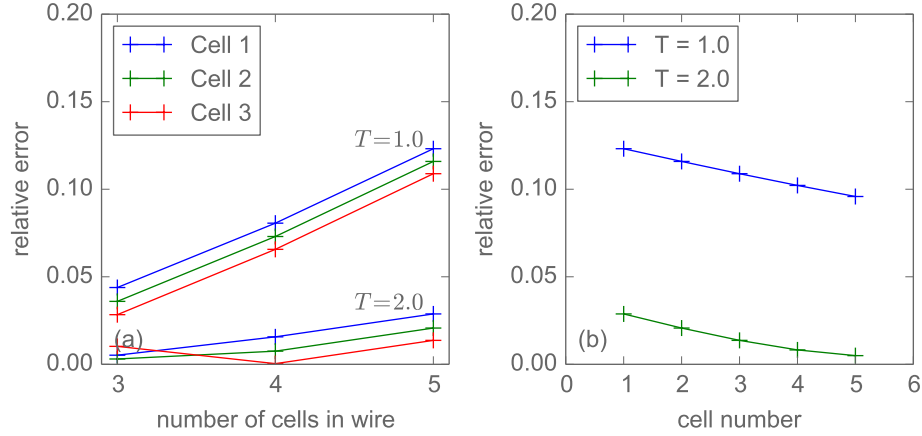
Figure 2.8: (a) The Ising model's relative error of the cell polarization for three-cell to five-cell charge-neutral wires at two different temperatures. The longer the wire the larger becomes the error. The error is no longer well controlled. (b) The Ising model's relative error for each cell's polarization in a five-cell charge-neutral wire. For the chosen parameters the error decreases along the wire. At least for the output polarization, the effect of a growing error with increasing wire length is therefore compensated.

cell inside a five-cell wire. Evidently, the error decreases along the wire and we can expect this decrease to counter the generally growing error for longer and longer wires, at least as long as we are mainly interested in the output polarization of the wire. However, this trend is not true generally, and for differently chosen system parameters the error may also remain constant along the wire. Still, for this particular QCA structure and for the chosen system parameters, we are relatively confident that the error of the output polarization, while not well controlled, will not grow very large for systems accessible with the Ising approximation—up two twelve QCA cells.

In this chapter we introduced and established three approximations for QCA systems: the fixed charge, the bond, and the Ising model. We usually use the fixed charge model as the starting point, without further explicit verification. In principle, whether the fixed charge approximation holds for a chosen set of parameters, has to be checked for each potential QCA implementation on a case by case basis. If the fixed charge model is not applicable, then there is also generally no hope of implementing QCA on the given experimental system. We generally assume doubly occupied states to be sufficiently gapped out and put U at infinity. The bond approximation is then a very good description of QCA systems at high temperatures. It starts breaking down when the temperature becomes comparable to the singlet-triplet splitting, and therefore for small V_1 and too large cell-cell distances. While it is conceptually deeply rewarding to map QCA to an Ising system, we

have seen the Ising approximation to be difficult to handle for practical calculations. It is only valid in a relatively small parameter window, at least for moderate system parameters, and great care has to be taken with its application. Generally speaking, both the bond and the Ising approximation become exact in the same limits—large V_1/t and small (but not too small) cell-cell distances. Not coincidentally, those are the limits where the QCA approach works best, as we will find out in the next chapter. Both approximations are useless for low-temperature calculations and for ground state properties we thus have to rely on the fixed charge model, which, however, only allows system sizes of up to three cells. We will use the bond model for most of our QCA characterization work at finite temperature. With system sizes of up to six cells it already allows for some interesting insights. The Ising model is problematic and we will employ it sparingly and only to look at larger structures such as gates.

Bibliography

[1] C. S. Lent, P. D. Tougaw, W. Porod, and G. H. Bernstein, "Quantum cellular automata," *Nanotechnology* **4** (1993) 49.

[2] G. H. Bernstein, A. Imre, V. Metlushko, A. Orlov, L. Zhou, L. Ji, G. Csaba, and W. Porod, "Magnetic QCA systems," *Microelectronics Journal* **36** (2005) 619–624.

[3] C. S. Lent and P. D. Tougaw, "A device architecture for computing with quantum dots," *Proceedings of the IEEE* **85** (1997) 541–557.

[4] R. A. Wolkow, L. Livadaru, J. Pitters, M. Taucer, P. Piva, M. Salomons, M. Cloutier, and B. V. C. Martins, "Silicon Atomic Quantum Dots Enable Beyond-CMOS Electronics," *arXiv preprint arXiv:1310.4148* (2013) .

[5] J. L. Pitters, L. Livadaru, M. B. Haider, and R. A. Wolkow, "Tunnel coupled dangling bond structures on hydrogen terminated silicon surfaces," *The Journal of chemical physics* **134** (2011) 064712.

[6] J. Hubbard, "Electron correlations in narrow energy bands. III. An improved solution," *Proceedings of the Royal Society of London. Series A. Mathematical and Physical Sciences* **281** (1964) 401–419.

[7] C. S. Lent and P. D. Tougaw, "Lines of interacting quantum-dot cells: A binary wire," *Journal of Applied Physics* **74** (1993) 6227–6233.

[8] P. D. Tougaw, C. S. Lent, and W. Porod, "Bistable saturation in coupled quantum-dot cells," *Journal of Applied Physics* **74** (1993) 3558–3566.

[9] P. D. Tougaw and C. S. Lent, "Dynamic behavior of quantum cellular automata," *Journal of Applied Physics* **80** (1996) 4722–4736.

[10] H. Fehske, R. Schneider, and A. Weiße, *Computational Many-Particle Physics*. Lecture Notes in Physics. Springer, 2008. `http://books.google.ca/books?id=XlQIFiSk7A8C`.

[11] G. Tóth and C. S. Lent, "Role of correlation in the operation of quantum-dot cellular automata," *Journal of Applied Physics* **89** (2001) 7943–7953.

[12] M. Taucer, F. Karim, K. Walus, and R. A. Wolkow, "Consequences of many-cell correlations in treating clocked quantum-dot cellular automata circuits," *arXiv preprint arXiv:1207.7008* (2012) .

[13] B. Bauer, L. Carr, H. Evertz, A. Feiguin, J. Freire, S. Fuchs, L. Gamper, J. Gukelberger, E. Gull, S. Guertler, *et al.*, "The ALPS project release 2.0: open source software for strongly correlated systems," *Journal of Statistical Mechanics: Theory and Experiment* **2011** (2011) P05001.

[14] X. Gonze, B. Amadon, P.-M. Anglade, J.-M. Beuken, F. Bottin, P. Boulanger, F. Bruneval, D. Caliste, R. Caracas, M. Cote, *et al.*, "ABINIT: First-principles approach to material and nanosystem properties," *Computer Physics Communications* **180** (2009) 2582–2615.

[15] F. Perez and B. E. Granger, "IPython: a system for interactive scientific computing," *Computing in Science & Engineering* **9** (2007) 21–29.

[16] G. Guennebaud, B. Jacob, *et al.*, "Eigen v3." Http://eigen.tuxfamily.org, 2010.

[17] A. Alexandrescu, "Modern C++ design: generic programming and design patterns applied,".

[18] "Boost C++ Libraries." `http://www.boost.org`.

[19] E. Jones, T. Oliphant, P. Peterson, *et al.*, "SciPy: Open source scientific tools for Python," 2001–. `http://www.scipy.org/`.

[20] J. D. Hunter, "Matplotlib: A 2D graphics environment," *Computing in Science & Engineering* **9** (2007) 0090–95.

[21] B. Ritter, "QCA TODO," 2014.

[22] B. Ritter, "Coma: A small Python library aiding with some aspects of running computer simulations," 2014. `https://github.com/meznom/coma`.

[23] A. W. Sandvik, "Stochastic series expansion method for quantum Ising models with arbitrary interactions," *Phys. Rev. E* **68** (Nov, 2003) 056701. `http://link.aps.org/doi/10.1103/PhysRevE.68.056701`.

[24] A. Auerbach, *Interacting electrons and quantum magnetism*. Graduate texts in contemporary physics. Springer New York, 1994. `http://books.google.ca/books?id=tiQlKzJa6GEC`.